CHARACTERIZATION OF MIXING IN T- AND Y-SHAPED MIXING CHAMBERS USING COMPUTATIONAL FLUID DYNAMICS

Aimée Tan

Master's thesis

Delft University of Technology
Department of Applied Physics

Delft, June 2002

Kramers Laboratorium voor
Fysische Technologie
Prins Bernhardlaan 6
2628 BW Delft

Professors:	Prof. dr. ir. H.E.A. van den Akker
	Prof. dr. ir. P.J. Jansens
Supervisors:	Dr. ir. J.J. Derksen
	Ir. C.P.M. Roelands

Acknowledgements

During the eight months that I worked on this project, I had help of a lot of people that I would like to thank. First of all, my supervisors Jos Derksen and Mark Roelands for their help during the project, especially for their patience during the last few days. When I had problems with Fluent, I had a lot of help from Niels van Wageningen and Frank Busing. Then I would like to thank Bas Rijkse for his feedback and Sander Jansz for helping me with C++. Of course I would like to thank Prof. Van den Akker and Prof. Jansens for making it possible to do my graduation project at their sections.

Abstract

In this research project, two mixer types were compared: a T-shaped mixer and a Y-shaped one. The mixers will be used in precipitation experiments where it is important to achieve fast micromixing. By using CFD (computational fluid dynamics) simulations, the mixers were characterized. The flow in the mixers was turbulent; the Reynolds number at the inlet was 9,000 and at the outlet it was 18,000.

First the simulation data of a straight pipe with a Reynolds number of 9,000 were compared to literature to validate the simulation method. Then simulations with the mixers were performed. The velocity field, kinetic energy and energy dissipation profiles for the mixers were compared. Also a model for macromixing was used and the concentrations of species A and B were calculated. The simulations show that macromixing is not yet completed at the outlet.

To check whether mixing on molecular scale was good or not, mixing times were calculated, both being dependent on the energy dissipation. Particle tracking was performed to obtain a history of the energy dissipation rates along their flow trajectories. The energy dissipation histories could be translated to these mixing times. Mixing times are a measure for the level of mixedness.
Two mixing time equations were used and compared to the residence time in the reactor.

List of symbols

Roman Symbols

Symbol	Description	S.I. units
c	Concentration	kg· m^{-3}
C	Mean concentration	kg· m^{-3}
C_D	Drag coefficient	-
$C_{1\epsilon}$	Empirical constant in k-ϵ model	-
$C_{2\epsilon}$	Empirical constant in k-ϵ model	-
C_μ	Dimensionless constant	-
d	Pipe diameter	m
D_p	Diameter of particle	m
$\mathbb{D}$	Diffusion coefficient	$m^2 \cdot s^{-1}$
E	Constant	-
f	Friction factor	-
F_D	Drag force per unit particle mass	m· s^{-2}
g	Gravitational force	m· s^{-2}
I	Turbulence intensity	%
J	Mass diffusion	kg· $m^{-2}s^{-1}$
k	Kinetic energy per unit mass	m^2s^{-2}
k^+	Normalized kinetic energy	-
l	Turbulence length scale	m
l_m	Mixing length	m
L	Pipe length	m
L	Length scale particle trajectory	m
m	Mass fraction	-
n	Exponential factor	-
N	Total number of species	-
P	Mean pressure	Pa
p	Pressure	Pa
r	Radial location in pipe	m
R	Radius of pipe	m
R	Reaction rate	kg· m^{-3} s^{-1}
S	Rate of creation by certain defined sources	kg· m^{-3} s^{-1}

t	Time	s
t_e	Engulfment time	s
t_h	Homogenization time	s
t_m	Micromixing time	s
T	Temperature	K
u	Velocity	$\mathrm{m{\cdot}s^{-1}}$
u_τ	Wall shear stress velocity	$\mathrm{m{\cdot}s^{-1}}$
u'	Turbulent velocity fluctuation	$\mathrm{m{\cdot}s^{-1}}$
u^+	Dimensionless near wall velocity	-
U	Time-smoothed average velocity	$\mathrm{m{\cdot}s^{-1}}$
U^+	Dimensionless velocity	$\mathrm{m{\cdot}s^{-1}}$
v	velocity (in y-direction)	$\mathrm{m{\cdot}s^{-1}}$
w	Velocity (in z-direction)	$\mathrm{m{\cdot}s^{-1}}$
y^+	Dimensionless distance from wall	-

Greek Symbols

Symbol	**Description**	**S.I. units**
β	Constant	
ϵ	Energy dissipation rate	$\mathrm{m^2s^{-3}}$
ϵ^+	Normalized dissipation rate	-
μ	Dynamic viscosity	$\mathrm{kg{\cdot}m^{-1}s^{-1}}$
κ	Von Kármán constant	-
λ	Kolmogorov thickness	m
μ_t	Eddy viscosity	$\mathrm{kg{\cdot}m^{-1}s^{-1}}$
ν	Kinematic viscosity	$\mathrm{m^2s^{-1}}$
ϕ	Variable	-
ρ	Density of fluid	$\mathrm{kg{\cdot}m^{-3}}$
σ_k	Prandtl number (k-ϵ model)	-
σ_ϵ	Prandtl number (k-ϵ model)	-
τ_w	Wall shear stress	$\mathrm{kg{\cdot}m^{-1}s^{-2}}$
ϑ	Velocity scale	$\mathrm{m{\cdot}s^{-1}}$

Subscripts

Abbreviation	**Description**
A	species A
B	species B

cl	centerline
in	condition at inlet
i	in i-direction
j	in j-direction
max	maximum
nb	neighboring
p	particle
P	cell
t	turbulent
α	species

Superscripts

Abbreviation	Description
’	fluctuating

Abbreviations

Abbreviation	Description
CFD	Computational Fluid Dynamics
DNS	Direct Numerical Simulation
UDF	User Defined Function

Dimensionless Numbers

Number	Description	Definition
Re	Reynolds number	$\rho u D/\mu$
Sc	Schmidt number	$\nu/\mathbb{D}$
Sc_t	Turbulent Schmidt number	$\mu_t/(\rho\mathbb{D})$

Contents

Chapter 1

Introduction

Many industrial products are formed by crystallization like pigments and pharmaceutical compounds. Understanding mixing properties is important when you want to investigate precipitation of particles, because reaction conditions have a great influence on the shape and size of precipitated particles. It is desired to have process control over these properties.

1.1 Precipitation

Precipitation is the process of formation of precipitates from a solution. It consists of two processes: nucleation and crystal growth. Nucleation is a dynamic process; constantly molecules of the insoluble product form clusters and break apart again. Only if a cluster exceeds a certain critical size, it will grow to form a crystal. The rate at which this happens is called the nucleation rate. Crystal growth is a dynamic process as well with molecules attaching to the cluster and breaking apart again. The rate at which a crystal grows is called the growth rate. Because of the statistical nature of the nucleation process, some time expires before nucleation takes place. This time can be very small, because the nucleation process increases exponentially with increasing supersaturation.
These processes determine the number and size of the crystals formed, the crystal size distribution. The crystal size distribution is very important for the properties of crystalline products. Therefore it is desired to have process control over these properties.

Both nucleation and growth depend on the supersaturation of the system. Supersaturation is expressed as the deviation of the concentration of the species from its equilibrium concentration. Supersaturation can be created in different ways:

- by reaction of two soluble compounds to an insoluble product, e.g. the reaction of H_4EDTA from a solution of its sodium salt with sulphuric acid:

$$4\ H^+(aq) + EDTA^{-4}(aq) \longrightarrow H_4EDTA(s)$$

- by addition of an anti-solvent to the solution, e.g. the precipitation of sodium chloride from its solution by mixing with ethanol.

Polymorphism is the case when one molecular compound is able to form more than one crystal structure. Under a given set of conditions, only one structure is stable, the others are metastable. The structure of the crystal determines product properties such as color in pigments and solubility in pharmaceutical compounds. Therefore it is of great interest for industry. Kinetics (i.e. nucleation and growth rates) may favor the formation of the metastable form over the stable one.

1.2 Setup of Polymorphism Project

The objective of the polymorphism project is to understand and if possible control the formation of polymorphic structures as a function of supersaturation. The method applied requires the reacting solutions to be completely mixed before the nucleation process starts. This means that mixing times must be very small, in the order of milliseconds.

A mixing chamber in which fast micromixing takes place is needed, because it will be used for kinetics measurements for precipitation reactions. Substances that will be used are for example EDTA (Ethylene Disodium Diamine Tetra Acetate) and L-glutamic acid. These precipitation reactions are very fast, because high supersaturations are used.

Fast precipitation reactions require fast mixing, therefore a mixing chamber that does not influence crystal properties in the succeeding precipitation reactions has to be designed. CFD simulations are used to quantify these. Below, a schematic drawing is given of the setup of these precipitation experiments.

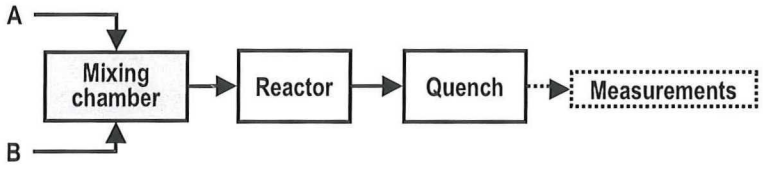

Figure 1.1: Setup of Precipitation Project

The ideal course is as follows. First two reactants, A and B, dissolved in a solvent are injected into the mixing chamber. Homogeneous mixing is achieved when micromixing is faster than the nucleation time. A and B react to an insoluble product, which gives the required supersaturation. In the reactor the reaction product starts to nucleate and grow under homogeneous conditions. After the reactor, the mixture is quenched to stop nucleation and growth. Then analysis of the obtained crystals

can be performed e.g. particle counting. If A and B mix homogeneously, the time for nucleation and growth is exactly known (the residence time in the reactor) and controllable by the length of the reactor. From the shift in the crystal size distribution with increasing residence time, the nucleation and growth rates will be calculated. This thesis will concentrate on the mixing chamber.

1.3 T and Y Mixers

In [Tan, 2001] an overview of different types of mixing chambers is given. The types of mixing chambers vary from two-impinging jets to a vortex mixer. In this research project, a mixing chamber with a short mixing time is required. It was decided to use the T- and Y-mixer, because of their low mixing times and simple geometry. These are mixers with similar geometry. A schematic drawing of the mixers is shown in figure 1.2. The difference between a T- and a Y-mixer is the angle α. For a T-mixer α is 0°, for a Y-mixer α is larger than 0°. The mixers have two inlets where the reactants are injected. Inside the mixer, the reactants mix and a mixture leaves the mixer from the outlet pipe. Many variations are possible in diameter, shape and length of the pipes. Here round pipes were chosen, because it is the most simple shape.

T- or Y-mixers are often used in precipitation experiments where two reactants are mixed in this type of mixer, before reacting and precipitating ([Mohanty et al., 2000],[Ståhl et al., 2001], [Manth et al., 1996], [Eble, 2000]).

It is interesting to compare the results for different angles α on the quality of mixing. In this thesis, a T-mixer will be compared with a Y-mixer, because it is not clear what influence the angle has on mixing. For the Y-mixer, an angle α of 10° was chosen, following [Eble, 2000].

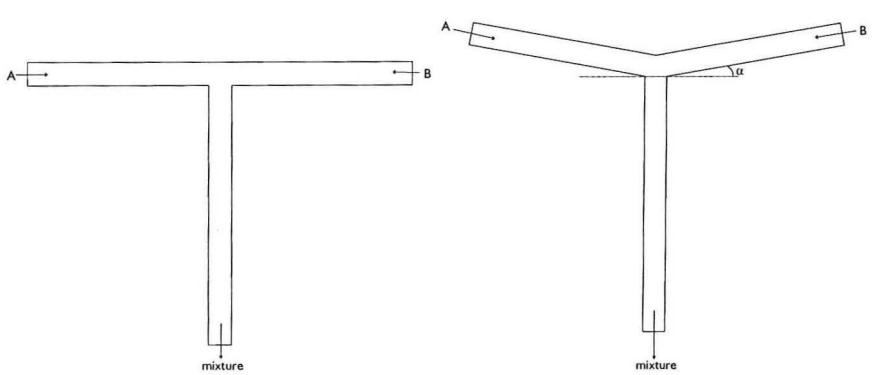

(a) T-shaped (b) Y-shaped, with angle α

Figure 1.2: T- and Y-mixer

1.4 Outline of the thesis

In the next chapter theory about turbulent flow will be discussed, as well as the different aspects of computational fluid dynamics (CFD). A discussion about different time scales will follow. In chapter 3, the setup of the CFD simulations will be explained, followed by the results and discussion in chapter 4. The last chapter contains the conclusions and recommendations for future work.

1.5 Project goals

For the precipitation project a fast mixing chamber is needed for mixing and reaction preceding the nucleation of crystals. T- and Y-mixers were selected for this. The aim of this graduation project is to characterise T- and Y-mixers for an experimental setup to study nucleation rates of precipitation processes.

Chapter 2

Theory

This chapter will describe the theory concerning flow in straight pipes, especially turbulent flow, the background of CFD and the models used in the simulations.

2.1 Governing Equations of Fluid Flow

In this section a mathematical basis for a general model for fluid flow will be discussed. It is based on the basic conservation laws of physics and leads to the governing equations of fluid flow. ([Nieuwstadt, 1998], [Versteegh and Malalasekera, 1998])

The continuity equation is based on the law of conservation of mass, which states that the mass of a fluid is conserved.

$$\frac{\partial \rho}{\partial t} + \frac{\partial \rho u_i}{\partial x_i} = 0 \tag{2.1}$$

Here, ρ is fluid density, $u_i$is velocity in direction i, x_i is the direction and t is time. In the equation above, like in the rest of this thesis, the Einstein convention is used, which means that a repeated index indicates that there is summed in all coordinate directions, for example: $u_i u_i = u_1 u_1 + u_2 u_2 + u_3 u_3$.In this thesis, a Cartesian coordinate system is used.

For an incompressible fluid, the density is constant and the continuity equation becomes:

$$\frac{\partial u_i}{\partial x_i} = 0 \tag{2.2}$$

Newton's second law of motion states that the rate of change of momentum of a fluid particle is the sum of forces on this particle. From this law, the momentum equations for three dimensions are derived, the so-called Navier-Stokes equations. These equations are valid for a Newtonian incompressible fluid. The Navier-Stokes

equation with negligible influence of gravitation is

$$\rho\frac{\partial u_i}{\partial t} + \rho u_j\frac{\partial u_i}{\partial x_j} = -\frac{\partial p}{\partial x_i} + \mu\frac{\partial^2 u_i}{\partial {x_j}^2} \tag{2.3}$$

where p is pressure and ν the kinematic viscosity. This is the dynamic viscosity μ over density: $\nu = \mu/\rho$.

The Reynolds number Re gives an indication of the importance of inertia forces (associated with convective effects) and viscous forces.

$$Re = \frac{\rho u d}{\mu} = \frac{u d}{\nu} \tag{2.4}$$

In experiments it is observed that at low Reynolds numbers, the flow is smooth and adjacent layers of fluid slide past each other in an orderly way. This is called the laminar regime. Laminar flows are completely described by the equations mentioned above. The continuity and Navier-Stokes equations form a closed set of equations with four unknowns: three velocities u_i, and pressure p.

For pipe flow, the character of the flow changes when Re is larger than approximately 2000. A complicated series of events takes place, where the flow becomes random and chaotic. At any point, the 3D velocity varies with both time and space. This is turbulent flow. The random nature of turbulent flow makes it very difficult to base computations on a complete description of the motion of all fluid particles. Instead, it is more attractive to describe turbulence by mean flow properties. The fluid velocity can be decomposed (Reynolds decomposition) in a steady mean value U and a fluctuating component $u_i'(t)$.

$$u_i(t) = U + u_i'(t) \tag{2.5}$$

The pressure can be decomposed in the sum of a mean and fluctuating component as well: $p = P + p'$. It is assumed that the fluctuations are continuous in both time and space. The decomposition leads to the following averaged continuity equation:

$$\frac{\partial U_i}{\partial x_i} = 0 \tag{2.6}$$

and the following Navier-Stokes equation:

$$\rho\frac{\partial \overline{U_i}}{\partial t} + \rho\frac{\partial U_i U_j}{\partial x_j} + \frac{\partial \overline{u_i' u_j'}}{\partial x_j} = -\frac{\partial P}{\partial x_i} + \mu\frac{\partial^2 U}{\partial {x_j}^2} \tag{2.7}$$

In this equation, a new term appears: $\overline{u_i' u_j'}$. This term contains six additional stresses (three normal stresses and three shear stresses), which are called the Reynolds stresses. These Reynolds stresses have to be predicted by turbulence modelling.

Below, two characteristics for turbulent flow are given. The turbulent kinetic energy per unit mass k is defined as:

$$k = \frac{1}{2}\overline{u_i'^2} \tag{2.8}$$

The turbulence intensity I is defined as the ratio of the root-mean-square of the velocity fluctuations to the mean flow velocity. It is a measure for the magnitude of the velocity fluctuations about the mean value. For a fully-developed duct flow, it is linked to kinetic energy and Re as follows [FluentInc., 1998]:

$$I \equiv \frac{\sqrt{\overline{u'^2}}}{U} = \frac{(\frac{2}{3}k)^{1/2}}{U} \cong 0.16(Re)^{-1/8} \tag{2.9}$$

Usually it is expressed as a percentage.

2.2 k-ϵ Model

In this section a commonly used turbulence model to predict the Reynolds stresses from the previous section will be discussed. It is called the k-ϵ model. This model is based on model transport equations for the turbulent kinetic energy and its dissipation rate. In the derivation of the k-ϵ model it was assumed that the flow is fully turbulent and the effects of molecular viscosity are negligible. Therefore, this model is only valid for fully developed turbulent flows.

The following model transport equations for k and ϵ are used [Versteegh and Malalasekera, 1998]:

Turbulent kinetic energy:

$$\rho\frac{\partial k}{\partial t} + \rho U_i\frac{\partial k}{\partial x_i} = \frac{\partial}{\partial x_i}\left(\frac{\mu_t}{\sigma_k}\frac{\partial k}{\partial x_i}\right) + \mu_t\left(\frac{\partial U_j}{\partial x_i} + \frac{\partial U_i}{\partial x_j}\right)\frac{\partial U_j}{\partial x_i} - \rho\epsilon \tag{2.10}$$

Dissipation Rate:

$$\rho\frac{\partial \epsilon}{\partial t} + \rho U_i\frac{\partial \epsilon}{\partial x_i} = \frac{\partial}{\partial x_i}\left(\frac{\mu_t}{\sigma_\epsilon}\frac{\partial \epsilon}{\partial x_i}\right) + C_{1\epsilon}\left(\frac{\epsilon}{k}\right)\mu_t\left(\frac{\partial U_j}{\partial x_i} + \frac{\partial U_i}{\partial x_j}\right)\frac{\partial U_j}{\partial x_i} - C_{2\epsilon}\rho\frac{\epsilon^2}{k} \tag{2.11}$$

In words these equations are:

Rate of change	+	Transport by convection	=	Transport by diffusion	+	Rate of production	-	Rate of destruction

The model constants in these equations are σ_k, σ_ϵ, $C_{1\epsilon}$ and $C_{2\epsilon}$. The eddy viscosity or turbulent viscosity μ_t is specified with help of the mixing length approach. In this approach, k and ϵ are used to define velocity scale ϑ and length scale l:

$$\vartheta = k^{1/2}, \qquad l = \frac{k^{3/2}}{\epsilon} \tag{2.12}$$

The turbulence length scale l is a physical quantity related to the size of the large energy-containing eddies.

The eddy viscosity is then specified as follows:

$$\mu_t = C_\mu \rho \vartheta l = \rho C_\mu \frac{k^2}{\epsilon} \tag{2.13}$$

where C_μ is a constant.

The five adjustable emipirical constants of the k-ϵ model have the following values.

$$\sigma_k = 1.00, \quad \sigma_\epsilon = 1.30, \quad C_{1\epsilon} = 1.44, \quad C_{2\epsilon} = 1.92, \quad C_\mu = 0.09.$$

These values are determined by data fitting for a wide range of turbulent flows. σ_k and σ_ϵ are the Prandtl numbers that connect the diffusivities of k and ϵ to the eddy viscosity μ_t.

2.3 Pipe Flow

Turbulent properties of pipe flow are considerably influenced by the presence of walls. In the center, inertia forces dominate the flow. The flow depends on the free stream parameters. Closer to the wall, viscous forces will be of the same magnitude or larger than inertia forces. Here, the flow is influenced by viscous effects rather than by the free stream parameters.

Figure 2.3 shows a schematic drawing of a pipe.

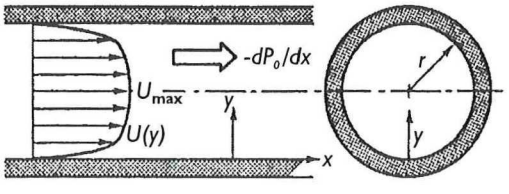

Figure 2.1: Turbulent pipe flow.

The mean velocity profile is determined experimentally and is given roughly by [Bird et al., 1960]:

$$\frac{U}{U_{max}} = \left(1 - \frac{r}{R}\right)^{1/n} \tag{2.14}$$

R is the radius of the pipe and r is the distance from the centerline. The exponential factor n depends on the Reynolds number. It is 6 for Re near 4,000 and 7 near 110,000. U_{max} represents the maximum mean velocity, in a pipe this is the centerline velocity.

2.3.1 Near Wall Velocity Profile

The mean flow velocity in the near wall region depends on the distance y from the wall, fluid density ρ, viscosity μ and wall shear stress τ_w.

Two important dimensionless groups that describe the near wall reagion are u^+ and y^+. The dimensionless near wall velocity u^+ is

$$u^+ = \frac{U}{u_\tau} \tag{2.15}$$

and the dimensionless distance from the wall is

$$y^+ = y\frac{u_\tau}{\nu} \tag{2.16}$$

Both dimensionless groups are scaled with the wall friction velocity, u_τ. It is also known as wall shear stress velocity.

$$u_\tau = \sqrt{\frac{\tau_w}{\rho}} \tag{2.17}$$

The wall shear stress τ_w is given as follows

$$\tau_w = \frac{1}{2}R \cdot \frac{\partial P}{\partial x} \tag{2.18}$$

In figure 2.2 the subdivisions of the near-wall region are illustrated in semi-log coordinates.

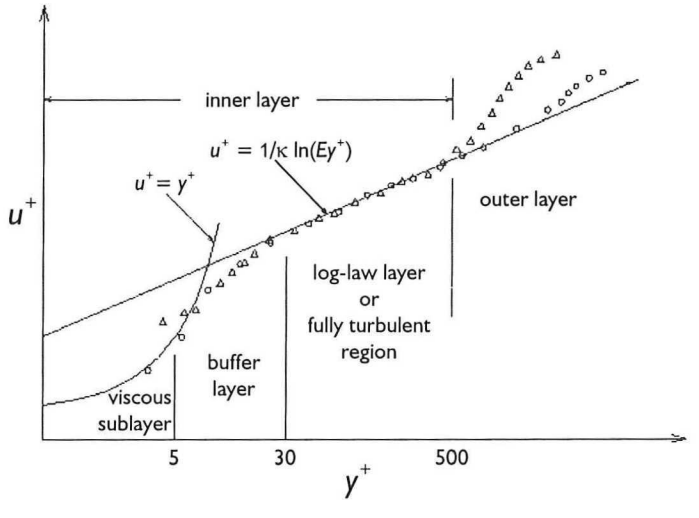

Figure 2.2: Subdivisions of the near-wall region (source: Fluent Inc.)

From left to right these regions are:

Viscous sublayer or linear sublayer ($y^+ < 5$)
Nearer to the wall, the eddy viscosity (equation 2.13) gets smaller, until it is in the

same range as the kinematic viscosity ν. This means that viscous effects dominate in this region. There is a linear relationship between velocity and the distance from the wall: $u^+ = y^+$.

Log-law layer or fully turbulent layer ($30< y^+ < 500$)
In this layer, eddy sizes are limited by the influence of the wall. Viscous and turbulent stresses are equally important. The mixing length is assumed to be $l = \kappa y$, which leads to the following profile: $u^+ = 1/\kappa \ln(Ey^+)$, where E is a constant ($= 9.8$) and κ is the Von Kármán constant ($= 0.41$), both values are determined experimentally. The law is called log-law, because of the logarithmic relationship.

Outer layer or fully turbulent layer ($y^+ > 500$)
In this region, the viscous stresses are negligible compared to the Reynolds stresses. Eddies are scaled with the geometry of the flow: $l = \beta R$, where β is a constant. In this layer, the velocity profile is described by the velocity-defect law:

$$\frac{U_{max} - U}{u_\tau} = \frac{2}{3\beta} \ln\left(1 - \frac{r}{R}\right)^{3/2} \tag{2.19}$$

The inner layer as shown in figure 2.2 consists of three zones: the first two layers discussed above and a buffer layer, which is located between these two layers. The thickness of the inner layer is 10–20 % of the total thickness of the wall layer. The shear stress is almost constant and equal to the wall shear stress in the whole inner region.

In modeling there are two methods to approach the near-wall region. In the near-wall model approach, the near-wall region is resolved all the way down to the wall with modified turbulence models valid in the wall region and a sufficiently small mesh. Alternatively, the near-wall region can be approached with wall functions. This approach bridges the viscosity-affected region with semi-empirical formulas. This option saves computational resources, is robust and is reasonably accurate.

In this thesis the standard wall functions are used. In standard wall functions the law-of-the-wall for mean velocity is:

$$U^* = \frac{1}{\kappa} \ln(Ey^*) \tag{2.20}$$

where

$$U^* \equiv \frac{U_P C_\mu^{1/4} k_P^{1/2}}{\tau_w/\rho} \tag{2.21}$$

and

$$y^* \equiv \frac{\rho C_\mu^{1/4} k_P^{1/2} y_P}{\mu} \tag{2.22}$$

and U_P the mean velocity of the fluid at point P, k_P the kinetic energy at point P and y_P the distance from point P to the wall. In Fluent [?] this law will be employed when $y^* > 11.225$. When y^* is smaller, the laminar stress-strain relationship is used:

$$U^* = y^* \tag{2.23}$$

As can be seen, Fluent uses the wall unit y^*rather than y^+. In equilibrium turbulent boundary layers they are approximately equal.

The k-equation is solved in the whole domain, including the wall-adjacent cells. The boundary condition for k at the wall is

$$\frac{\partial k}{\partial n} = 0 \tag{2.24}$$

where n is the local coordinate normal to the wall.
The production G_k and dissipation of kinetic energy are computed on the basis of the local equilibrium hypothesis. This hypothesis states that in the wall-adjacent control volume, production of k and its dissipation rate are equal. The production of k is computed from

$$G_k \approx \tau_w \frac{\partial U}{\partial y} = \tau_w \frac{\tau_w}{\kappa \rho C_\mu^{1/4} k_P^{1/2} y_P} \tag{2.25}$$

and ϵ from

$$\epsilon_P = \frac{C_\mu^{3/4} k_P^{3/2}}{\kappa y_P} \tag{2.26}$$

Equation 2.26 is used for calculating ϵ at the wall adjacent cells.

2.3.2 Profiles in Fully Developed Turbulent Flow

The boundary conditions of the flow in the mixer inlets were of fully turbulent pipe flow. In this section, the equations used to describe those boundary conditions, are given.

The velocity profile can be described with equation 2.14.

The turbulent kinetic energy is assumed to vary linearly from a near wall value of

$$k_{nw} = \frac{u_\tau^2}{\sqrt{C_\mu}} \tag{2.27}$$

to a centerline value of

$$k_{cl} = 0.002 U_{max}^2 \tag{2.28}$$

The dissipation rate is given by

$$\epsilon = C_\mu^{3/4} \frac{k^{3/2}}{l} \tag{2.29}$$

The mixing length is the minimum of κy (in the log-law layer) and $0.085R$ (in the outer layer).

For a fully developed turbulent flow, the wall shear stress can be written as follows:

$$\tau_w = \frac{f \rho U_{max}^2}{2} \tag{2.30}$$

where the friction factor f is estimated from the Blasius equation:

$$f = 0.045 \Big(\frac{U_{max} R}{\nu} \Big)^{-1/4} \tag{2.31}$$

2.4 Species Diffusion

The species mass fractions are predicted by the conservation equation for the α'th species [FluentInc., 1998]:

$$\frac{\partial}{\partial t}(\rho m_\alpha) + \frac{\partial}{\partial x_i}(\rho u_i m_\alpha) = -\frac{\partial}{\partial x_i} J_{\alpha,i} + R_\alpha + S_\alpha \tag{2.32}$$

where m_α is the mass fraction of α.

$J_{\alpha,i}$ is the mass diffusion in turbulent flow:

$$J_{\alpha,i} = -\big(\rho \mathbb{D}_{\alpha,m} + \frac{\mu_t}{Sc_t}\big) \frac{\partial m_\alpha}{\partial x_i} \tag{2.33}$$

where $\mathbb{D}_{\alpha,m}$ is the diffusion coefficient of species α in the mixture and Sc_t is the turbulent Schmidt number:

$$Sc_t = \frac{\mu_t}{\rho \mathbb{D}_t} \tag{2.34}$$

Default Sc_t is set to 0.7. μ_t is the turbulent or eddy viscosity as given in equation 2.13.

$R_{i'}$ is the reaction rate and $S_{i'}$ is the rate of creation by other sources. The latter two terms are not used in the simulations done for this thesis. The species diffusion is solved for $N - 1$ species, where N is total number of fluid phase chemical species present. The species that is not solved is the solvent.

2.5 Computational Fluid Dynamics

Computational fluid dynamics (CFD) is used as an alternative for or complementary to experimental work. A computer calculates the flow in the system (e.g. a reactor) by calculating the applicable equations for fluid flow. In this thesis the CFD code Fluent [FluentInc., 1998] was used. Fluent uses the finite volume approach to solve the governing equations of conservation of mass, momentum and when applicable for energy and other scalars, like chemical species.

2.5.1 Why CFD?

CFD has several advantages compared to experimental work. With CFD it is possible to see what happens *inside* the system. This might not be visible through any other means. The user may specify different sets of circumstances, or different systems, without having to build an experimental setup. CFD predicts what will happen. Therefore it is possible to predict the performance of different systems under different circumstances in a short period of time. Nevertheless, often it is profitable to use simulations and experiments complementary. CFD uses model equations and the user has to do assumptions. Also in practice some unexpected events may occur that are not accounted for in the model. When performing experiments, the CFD calculations can be validated.

2.5.2 How does CFD work?

The following steps will be performed in a CFD simulation:

1. Construction of the geometry,
2. Division of the geometry in cells and grid points for discretization and computation,
3. Selection of the model (with governing equations),
4. Setting of the appropriate boundary conditions,
5. Selection of the numerical discretization schemes used to solve the governing equations, and
6. Iteratively solving the obtained set of equations for all grid points.

Fluent solves the governing equations for conservation of mass and momentum and for scalars such as turbulence and chemical species. Solving consists of the following steps.

- Division of the domain into discrete control volumes, using the computational grid defined by the user.
- Integration of the governing equations for the control volumes to construct algebraic relations for the unknowns (like velocity and pressure).
- Linearization of these discretized equations and solving them to acquire updated values of the dependent variables.

First steps 1 and 2 will be explained in paragraph 2.5.3. Then steps 3 and 4 will be explained in paragraph 2.5.4, and steps 5 and 6 in paragraph 2.5.5.

2.5.3 Construction and Division of Geometry

The geometry is constructed with help of Gambit 2.0.4 [FluentInc., 1998]. The mixers in this thesis are very simple geometries, consisting of two or three cylinders, interconnecting at a certain angle (90° for a T, 100° for a Y). See figure 2.3 for construction of T-mixer. First the cylinders are defined by specifying length, radius and direction (1–2). The cylinders are merged in the center to obtain one T-shaped structure (3). Because the mixer is symmetric, the rear part was deleted to obtain a half T-mixer with a symmetry plane at the back (4). This is done to save computer time in Fluent calculations.

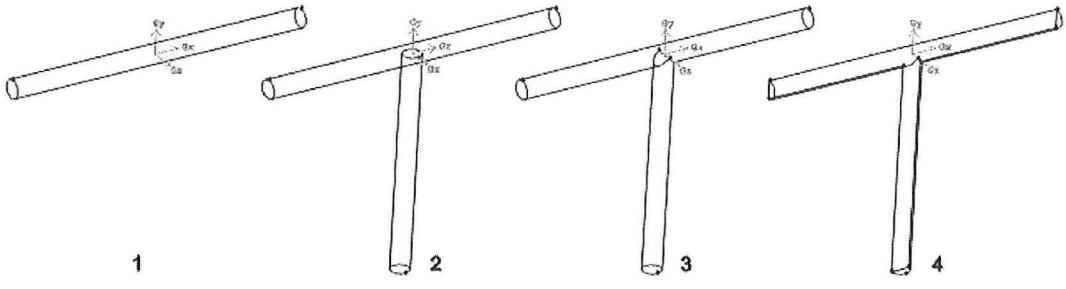

Figure 2.3: Subsequent steps in geometry construction.

The geometry shown in step 4 will be used for simulation. To make meshing possible in a structured way, this geometry was subdivided into several smaller parts. This is shown in figure 2.4 where the next steps are shown for part of the inlet pipe. As can be seen in (1), it is subdivided into several subdivisions with more or less the same shape. Then, the boundary layers were defined for the surfaces perpendicular to the flow (2). The boundary layers are needed for a nicer mesh near the walls. The third step is to mesh the edges, that means that the edges are divided into small pieces that are used to define the face mesh. The dots indicate the borders of those pieces and are called nodes. The face mesh is shown in (4). The fifth step is to use these face meshes to construct a volume mesh (5). Now this volume is divided into small volumes that are used for calculation by Fluent.

2.5.4 Boundary Conditions and Model Selection

Boundary conditions specify the flow variables on the boundaries of the model. The following boundary conditions can be specified:

- Inlet (e.g. velocity inlet or pressure inlet),
- Outlet (e.g. pressure outlet or outflow),
- Symmetry boundary conditions, and
- Axis boundary conditions.

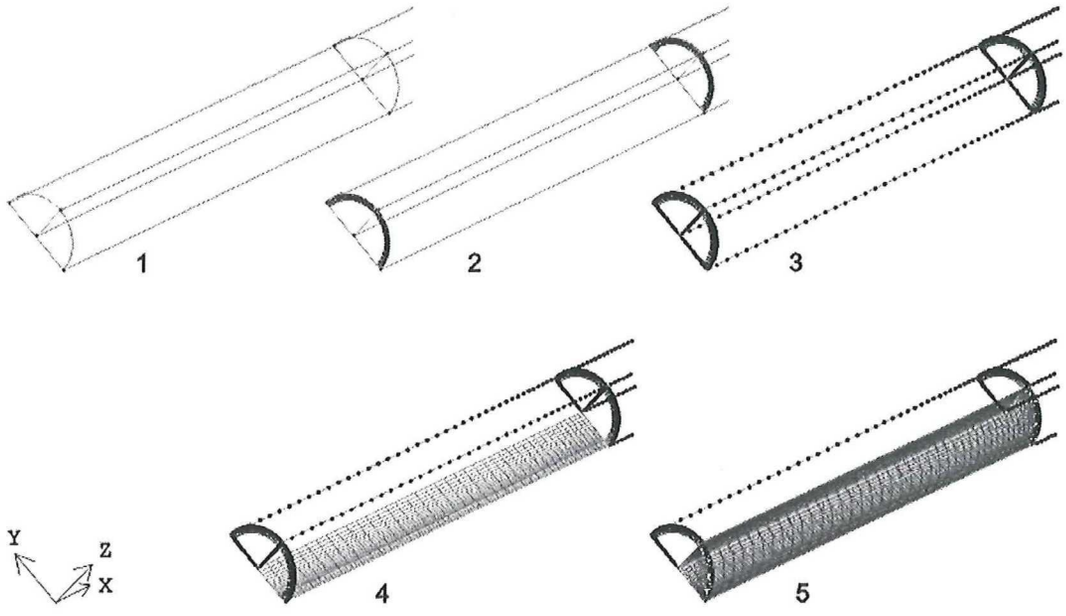

Figure 2.4: Subsequent steps in mesh construction.

The symmetry boundary condition can be used when the physical geometry of interest and the flow pattern have mirror symmetry. Fluent assumes a zero flux of all quantities across this boundary, so the normal gradients of all flow variables are zero. Also, zero normal velocity is assumed at the symmetry plane. The axis boundary condition must be used as the centerline of an axisymmetric geometry. In section 3.3 the properties of these boundary conditions will be explained more detailed.

The model selection depends on the physics encompassed in the flow, the experience with a specific class of problem, the level of accuracy required, the available computational resources, and the amount of time available for the simulation. ([FluentInc., 1998])

In this thesis the k-ϵ model was chosen, because it is a simple turbulent model, with only two equations, while the accuracy is reasonable. It is the most widely used model, which means that the strengths and weaknesses are well documented.

2.5.5 Model Solving

Fluent provides three different solvers: segregated, coupled implicit and coupled explicit. The difference between the segregated and coupled solver is the fact that the segregated solver solves the governing equations sequentially (segregated from each other) and the coupled solver solves them simultaneously (coupled together). The second difference is in the manner of linearization. In the implicit form, the unknown value of a given variable in each cell is computed using both existing and unknown values from neighboring cells. Therefore each unknown will appear in more

equations in the system and these equations must be solved simultaneously. In the explicit form, the unknown in each cell is computed with existing values only. Each unknown will appear in one equation only and the equation can be solved.
All solvers are accurate for a broad range of flows, but as the coupled solver originally was developed for high-speed compressible flows, it might give better performance in those cases.

Because in this thesis the segregated solver is used, only this one will be explained here. In the segregated solver, each discrete governing equation is linearized implicitly with respect top that equation's dependent variable, resulting in a system of linear equations with one equation for each cell. This is often called a 'scalar' system of equations, because there is only one equation per cell. The segregated approach solves a single variable field, e.g. p by considering all cells at the same time. Then it solves the next variable field.

A control-volume-based technique is used for converting the governing equations to algebraic equations that can be solved numerically. First, the governing equations are integrated about each control volume to yield discrete equations that conserve each quantity. This is illustrated by considering the steady-state conservation equation for transport of a scalar quantity ϕ for an arbitrary control volume V:

$$\oint \rho\phi\mathbf{v}d\mathbf{A} = \oint \Gamma_\phi \nabla\phi d\mathbf{A} + \int_V S_\phi dV \tag{2.35}$$

where $\mathbf{v}$ is the velocity vector, $\mathbf{A}$ the surface area vector, Γ_ϕ the diffusion coefficient for ϕ, $\nabla\phi$ the gradient of ϕ and S_ϕ the source of ϕ per unit volume. Equation 2.35 is applied to each control volume in the computational domain.
Discretization yields

$$\sum_f^{N_{\text{faces}}} v_f \phi_f A_f = \sum_f^{N_{\text{faces}}} \Gamma_\phi (\nabla\phi)_n A_f + S_\phi V \tag{2.36}$$

with N_{faces} the number of faces enclosing the cell, ϕ_f the value of ϕ convected through face f, v_f the mass flux through f, A_f the area of f, $(\nabla\phi)_n$ the magnitude of the gradient of ϕ normal to f and V the cell volume. The equations solved by Fluent have the same form as the one given above.

Because the governing equations are nonlinear, iteration is necessary for a converged solution. Each iteration step consists of successively updating of properties, solving of momentum equations, solving of pressure-correction such that continuity is satisfied, solving of scalar equations such as energy, species and turbulence and checking if convergence is achieved for the set of equations.

Convergence is monitored with the residual sum. this is defined below. After discretization, the conservation equation for a variable ϕ at a cell P is:

$$a_P \phi_P = \sum_{nb} a_{nb}\phi_{nb} + b \tag{2.37}$$

with a_P the center coefficient, a_{nb} the influence coefficients for the neighbouring cells and b is the contribution of the constant part of the source term and of the boundary conditions. The center coefficient a_P is

$$a_P = \sum_{nb} a_{nb} - S_P \tag{2.38}$$

The residual R^ϕ computed by Fluent is the imbalance of equation 2.37 summed over all computational cells P. It is often referred to as the 'unscaled' residual.

$$R^\phi = \sum_{\text{cells P}} \left| \sum_{nb} a_{nb}\phi_{nb} + b - a_P\phi_P \right| \tag{2.39}$$

In general, it is difficult to judge and compare convergence with the residuals of equation 2.39 as no scaling is employed. Therefore the residuals are scaled with a representative of the flow rate of ϕ through the domain. The 'scaled' residual is defined as

$$R^\phi = \frac{\Sigma_{\text{cells P}} |\Sigma_{nb} a_{nb}\phi_{nb} + b - a_P\phi_P|}{\Sigma_{\text{cells P}} |a_P\phi_P|} \tag{2.40}$$

For momentum equations, ϕ_P is replaced by u_P, the magnitude of velocity at cell P. For the continuity equation, the unscaled residual is defined as

$$R^c = \sum_{\text{cells P}} |\text{rate of mass creation in cell P}| \tag{2.41}$$

and the scaled residual as

$$\frac{R^c_{\text{iteration N}}}{R^c_{\text{iteration 5}}} \tag{2.42}$$

where the denominator ($R^c_{\text{iteration 5}}$) is the largest absolute value of the residual continuityequation in the first five iterations. It must be noted that a good first estimate will increase the scaled residual as the first five iterations are already close to the solution.

The default settings for the scaled residuals are 10^{-3}. If all the residuals are below this, the solution is considered to be converged. The convergence criteria can be adjusted for each variable.

2.5.6 Particle Trajectory Calculations

In order to learn more about properties of the simulated geometry, particle tracking may be a useful tool. Fluent calculates the trajectory of a particle injected at a certain location defined by the user. It may provide useful information about the flow field.
Particle tracking is a Discrete Phase modeling option in Fluent. These models are used for calculation of trajectories and other properties of a discrete phase (particles, droplets or bubbles dispersed in the continuous phase). In the simulations described

in this thesis, inert particles were used with no influence on the flow. First the continuous phase flow field is solved as described in the previous sections, then the particle trajectories are calculated.

First, the initial conditions for all dependent variables have to be set. The variables describe the conditions of an individual particle at injection point. The initial conditions that have to be set are: position (x, y and z-coordinate), velocities (u,v and w), diameter of the particle D_p and temperature of the particle T_p.

There are two types for particle trajectory calculations: coupled (including effects of particles on the continuous phase) and uncoupled (particles having no influence on the continuous phase). In this thesis, the uncoupled type was used. The particles injected in the simulations performed here, are injected to determine the properties of the flow field. In reality these particles are not present.

The calculation method is discussed here. The trajectories are calculated by integrating the force balance on each particle. The force balance in x-direction is written in Lagrangian (moving with particle) reference frame as follows

$$\frac{du_p}{dt} = F_D(u - u_p) + g_x\frac{\rho_p - \rho}{\rho_p} + F_x \tag{2.43}$$

where u_p is the particle velocity, u the fluid phase velocity, ρ_p the density of the particle and ρ the fluid density. g_x is the force of gravity in x-direction. In this thesis, this term is zero, because the particles have the same density as the fluid and the force of gravity is set to zero.
F_x is the term for other forces like virtual mass (needed when $\rho > \rho_p$) and Brownian forces. In this thesis, this term is zero as well.
F_D is the drag force per unit particle mass:

$$F_D = \frac{18\mu}{\rho_p D_p^2}\frac{C_D Re_p}{24} \tag{2.44}$$

D_p is the particle diameter, Re_p is the relative Reynolds number

$$Re_p = \frac{\rho D_p |u_p - u|}{\mu} \tag{2.45}$$

and C_D is the drag coefficient:

$$C_D = a_1 + \frac{a_2}{Re} + \frac{a_3}{Re^2} \tag{2.46}$$

where the a's are constants for smooth spherical particles for different Re_p's. These constants can be found in [Morsi and Alexander, 1972].

The trajectory equation and any auxiliary equations are solved by stepwise integration over discrete time steps. These time steps are defined by the user, who defines length scale L. The time step is then

$$\Delta t = \frac{L}{u_p + u_c} \tag{2.47}$$

where u_c is the velocity of the continuum.

Equation 2.43 yields the velocity of each particle at each point of the trajectory. The trajectory itself is calculated with:

$$\frac{dx}{dt} = u_p \tag{2.48}$$

These equations are solved simultaneously to determine the velocity and position of a particle.

For turbulent flows it is possible to use the stochastic tracking technique. This includes the effect of turbulent velocity fluctuations on the particle trajectories.

When a particle moves through the fluid it may meet boundaries. There are different ways of dealing with this: a particle may reflect against a wall, evaporate at a surface or escape through an outlet.

2.6 Time Scale Analysis

In Fluent, only dispersive mixing is taken into account (with Sc_t). Here mixing on smaller scales is also important. In this section different characteristic times on smaller scales are discussed. In literature, many approaches to define a micromixing time scale can be found.

Homogenization Time
[Corrsin, 1964] derived the following equation for micromixing.

$$t_h = \frac{3}{2}\frac{k}{\epsilon} + \frac{1}{2}\ln Sc\left(\frac{\nu}{\epsilon}\right)^{1/2} \tag{2.49}$$

It was derived as follows. The mass transfer equation is:

$$\frac{\partial c}{\partial t} + u_i\frac{\partial c}{\partial x_i} = \mathbb{D}\frac{\partial c}{\partial x_i} \tag{2.50}$$

The concentration can be written as the sum of the mean and fluctuating parts $c(x,t) = C + c'(x,t)$. There is statistical homogeneity in space so $C = C(t)$. Since there is no chemical reaction, C is constant and equation 2.50 reduces to:

$$\frac{\partial c'}{\partial t} + u_i\frac{\partial c'}{\partial x_i} = \mathbb{D}\frac{\partial c'}{\partial x_i} \tag{2.51}$$

Multiplying by c, averaging, using mass conservation to get u_i inside the derivative, and invoking homogeneity, equation 2.51 can be converted to:

$$\frac{\partial \overline{c'^2}}{\partial t} = -2\mathbb{D}\overline{\left(\frac{\partial c}{\partial x_j}\right)\left(\frac{\partial c}{\partial x_j}\right)} \tag{2.52}$$

The derivative products can be replaced by defining characteristic lengths, such that equation 2.52 can be written as:

$$\frac{\partial \overline{c'^2}}{\partial t} = -12\mathbb{D}\frac{c'^2}{l^2} \tag{2.53}$$

The following homogenization time t_h can be chosen:

$$t_h \equiv \frac{l^2}{12\mathbb{D}} \tag{2.54}$$

that is

$$\overline{c'^2}(t) = \overline{c_0^2} \exp\left[-\frac{t}{t_h}\right] \tag{2.55}$$

The following length scale was chosen:

$$l \approx 18 \frac{\left(\frac{k_K}{k_0}\right)^{2/3} + \frac{2}{3}\ln\left(\frac{k_B}{k_K}\right)}{k_B^2} \tag{2.56}$$

where k_K is the Kolmogorov wave number $= (\epsilon/\nu^3)^{1/4}$, k_B is the Batchelor wave number $= (\epsilon/(\nu\mathbb{D}^2))^{1/4}$ and k_0 the following wave number $k_0 = (\epsilon^{2/3}/k)^{3/2}$. Equation 2.49 follows from equation 2.54 and 2.56. It consists of two times: the first part k/ϵ is the eddy dissipation time and the second part gives diffusion (with Sc). The time scale has a weak dependency of Sc.

Micromixing Time

[Demyanovich and Bourne, 1989] used the following equation for micromixing time:

$$t_m = \frac{0.25}{\mathbb{D}}\left(\frac{\nu^3}{\epsilon}\right)^{1/2} = 0.25 \cdot Sc\left(\frac{\nu}{\epsilon}\right)^{1/2} \tag{2.57}$$

It is based on diffusion over half Kolmogorov thickness δ: $t_m = \delta^2/\mathbb{D}$. Kolmogorov thickness λ is considered the smallest length scale in turbulent flow.

$$\delta = 0.5\lambda = 0.5\left(\frac{\nu^3}{\epsilon}\right)^{1/4}$$

[Geisler et al., 1988] derived the following equation:

$$t_m = 50\left(\frac{\nu}{\epsilon}\right)^{1/2}(0.88 + \ln Sc) \tag{2.58}$$

It is based on the same length scale as [Corrsin, 1964] used (equation 2.56). In the derivation of this equation, a segregation index (a measure for local micromixing) was used. A fluid is considered homogenously mixed, when segregation is smaller than 1 %. The 50 in this equation results from that assumption.

Engulfment Time

[Bałdyga and Bourne, 2000] defined a different time scale, called the engulfment time t_e.

$$t_e = K\left(\frac{\nu}{\epsilon}\right)^{1/2} \tag{2.59}$$

with K a constant. The value of K is determined experimentally, and is 17.24 here [Shekunov et al., 2001]. In this theory, mixing processes occur on different scales. First dispersive mixing, where reactants are dispersed by large scale eddies. Then these large eddies disintegrate to smaller eddies. The final size of these eddies is the

Kolmogorov length. The process of engulfment takes place in the viscous-convective range (between Kolmogorov and Batchelor scale) and can be seen as the decay of the smallest eddy. According to [Shekunov et al., 2001] for $1 \ll Sc \ll 4000$, the viscous-convective engulfment controls mixing below the Kolmogorov microscale and effects of molecular diffusion are negligible.

Chapter 3

Numerical Simulations Setup

This chapter describes which simulations have been performed and what parameter settings have been used. First, the general parameters are given. Then, simulations in a straight pipe were done, to find out which boundary conditions were suitable for further simulations in mixing chambers. The setup and results of the pipe are given in the first sections. Then, the resulting boundary conditions for the mixing chamber simulations are given. In the last section, the settings for particle tracking are given.

3.1 Software and Hardware

For construction of the geometry and making of the grid, Gambit 2.0.4 was used. For simulations of the flow field, Fluent 6.0.20 was used. Both programs were running on a Unix system installed on a PC running Linux Red Hat 7.0. The computer was equipped with an AMD Athlon Thunderbird 1.33 GHz processor with available memory of 1024 MB.

3.2 Fluid Parameters

For the simulations, standard conditions for temperature (300 K) and pressure (101,325 Pa) were used.

The simulations were done with three different species: A, B and water. Water was the solvent, as it will be in the real experiments. A and B were model species, with the same properties as water and diffusion coefficients of the order of magnitude of the species that will be used in later experiments: $\mathbb{D} = 10^{-9}$ m^2s^{-1}. The properties of A, B and water are given in table 3.1.

The following boundary conditions are defined: the mean inlet velocity = 3 m/s,

Table 3.1: Properties of water, A and B

Property	Dimension
Density	998.2 $kg{\cdot}m^{-3}$
C_P	4182 $J\ kg^{-1}K^{-1}$
Thermal Conductivity	0.6 $W{\cdot}m^{-1}K^{-1}$
Viscosity μ	$1.003{\cdot}10^{-3}$ $kg{\cdot}m^{-1}s^{-1}$
Mass Diffusivity	10^{-9} m^2s^{-1}
Molecular weight	18.0152 $g{\cdot}mol^{-1}$

which means with a diameter of 3 mm, a Re_{in} of 9,000. Based on the centerline velocity in developed turbulent flow Re_{cl} = 10,800. The Schmidt number $Sc = \nu/\mathbb{D}$ is 1000. The convergence criteria for all properties were 10^{-5}.

3.3 Verification of Simulation with Pipe Flow

The flow of the mixer is in the turbulent regime, therefore the k-ϵ model could be used. There is a drawback, a Re of 9,000 is quite low for turbulent flow. It might be too low for simulations with a simple turbulence model. Therefore, before performing the simulations in the mixers, a simpler geometry, a straight pipe, was simulated and compared to literature data. This was done to find out which simulation properties were suitable for simulations. This section describes how this has been done. The simulations were tested on dependency of number of grid cells, dependency of outlet type and dependency of inlet conditions.

The pipe was chosen to have the same dimensions as the pipes in the mixer. This means a diameter of 3 mm. The length was chosen to be sufficiently long to achieve fully developed turbulent pipe flow: $35D$, which is equal to 105 mm. The inlet velocity was chosen to be a uniform velocity field of 3 m/s. It was decided to do the simulations in a quarter of a pipe (see figure 3.1), with two symmetry planes. Simulating only part of the geometry saves computer time and because of symmetry, the solution is the same as for a complete pipe.

3.3.1 Grid Sizes

To test grid independency, four different grids were constructed. The first three grids were constructed in three-dimensional mode, while the last grid was constructed axisymmetrically (with the x-axis as symmetry axis), a two-dimensional mode. One standard grid was chosen consisting of 56,400 cells. From this case a coarser version was made, and a finer one. The cross-sections of the three-dimensional grids are shown in figure 3.2. In this figure, the x-axis is located perpendicular to the y, z-plane. The x, y-planes and x, z-planes are the symmetry planes.

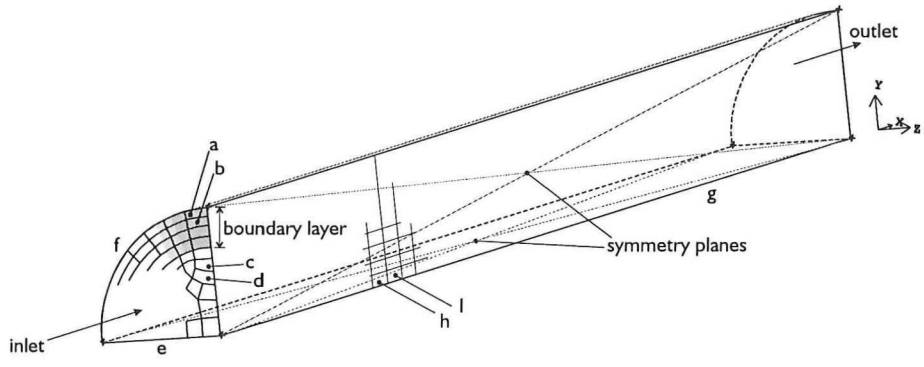

Figure 3.1: Geometry of the pipe (not to scale) with indicated: (a) first and (b) next layer in the boundary layer, (c) and (d) successive layers outside the boundary layer, (e) radius, (f) circumference, (g) length of the tube and (h) and (i) successive cells in lengthwise direction.

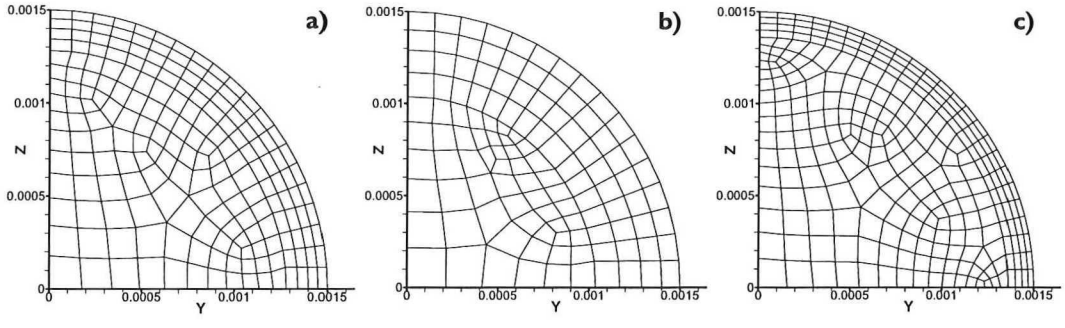

Figure 3.2: Cross-section of the grid at the inlet of the pipe, with different meshes: a) Standard, b) Coarse, c) Fine. The coordinates are given in meters.

The face meshes in figure 3.2 were obtained as follows: first the number of intervals on each line were defined, and a boundary layer was defined on the circumference. Then the face was meshed using the scheme 'Pave'. The axisymmetric grid consists of a two-dimensional mesh, which is the same as the symmetry plane of the standard grid. This mesh is shown in figure 3.3. After simulation, three-dimensional flow property profiles can be obtained by rotating this plane around the X-axis for 360°.

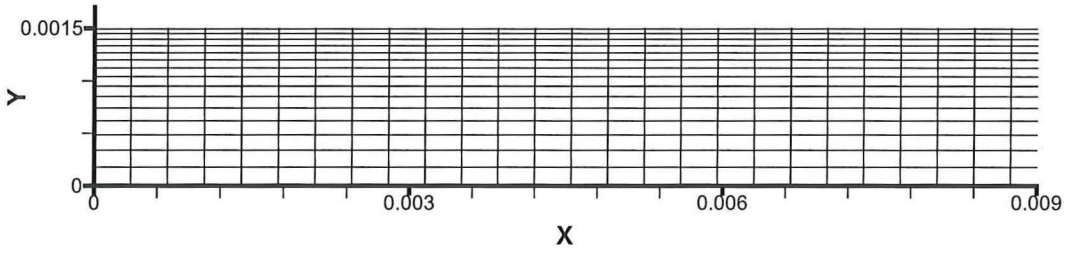

Figure 3.3: Lengthwise cross-section of pipe grid. For the sake of clarity only the first part is shown. The coordinates are given in meters.

The exact construction parameters are given in table 3.2. The growth factor gives the ratio of two successive cells. In figure 3.3 this are the ratios b/a for the boundary layer and d/c outside the boundary layer.

Table 3.2: Grid properties, see figure 3.1 for clarification of the letters.

	Standard	Coarse	Fine	Axisymmetric
Boundary layer				
- Size first layer (a) [mm]	0.05	0.1	0.03	0.05
- Growth factor (b/a)	1.1	1.1	1.1	1.1
- Number of layers	4	4	4	4
Number of cells				
- Radial (e)	15	10	20	15
◁ Growth factor (d/c)	1.1	1.1	1.1	1.1
- Circumferential (f)	20	16	24	n.a.
- Lengthwise (g)	300	230	370	300
Total number of cells	56,400	26,910	99,160	4,500

3.3.2 Types Of Turbulent Inlet Conditions

In Fluent there are different methods to specify the turbulent conditions in the velocity inlet. The turbulent conditions in the inlet of the flow entering the geometry depend on the upstream history of the flow. In this case, the flow is assumed to be turbulent when entering the mixer. The inlet pipe of the mixer has a length of 25 mm and for mixer simulations it is desired to have fully developed turbulent flow a small distance before impingement, which means after about 21 mm ($= 7D$). Here, two methods are compared: specifying kinetic energy and energy dissipation, and

specifying intensity and length scale.

The settings in inlet conditions A are the defaults of Fluent (see table 3.3).

Table 3.3: Inlet conditions A

Kinetic energy, k	1 m^2/s^2
Energy dissipation, ϵ	1 m^2/s^3

For case B, the turbulent intensity was estimated by equation 2.9. For a Reynolds number of 9,000, the intensity is 5 %. The length scale l was estimated by the approximate relationship between l and the size of the pipe: $l = 0.07D$ [FluentInc., 1998]. For a tube with an internal diameter of 3 mm, the length scale is 0.2 mm. (See table 3.4.)

Table 3.4: Inlet conditions B

Intensity, I	5 %
Length Scale, l	0.0002 m

3.3.3 Types of Outlet Conditions

There are two suitable types of outlet; the pressure outlet and an outflow. When using a pressure outlet, the static pressure has to be defined at flow outlets. When backflow occurs during iteration, a pressure outlet often results in a better convergence rate than an outflow. Outflow conditions can be used when the details of the flow velocity are not known. Its use is appropriate when the exit is close to a fully developed condition, as the outflow assumes a zero normal gradient for all flow variables except pressure.

For the pressure outlet the following parameters had to be specified: a gauge pressure of 101,325 Pa, the backflow properties were set the same as the corresponding inlet properties: a backflow turbulence intensity of 5 % and a backflow turbulence length of 0.0002 m.

3.3.4 Results and Conclusions

The results of the simulations with the conditions discussed above were compared to data from literature. The kinetic energy and velocity profiles were compared with DNS (direct numerical simulation) data of [Eggels et al., 1994], with a Re_{cl} of 7,000. The turbulent dissipation rate was compared to the DNS data of [Kim et al., 1987], with a Re_{cl} of 6,600. Both Re are based on centerline velocity U_{cl}: $Re = U_{cl}D/\nu$.

The turbulent properties were plotted against the distance from the centerline in the outlet of the pipe. This quantity was made dimensionless by dividing by the radius: r/R. The turbulent properties were made dimensionless as well. The velocity, kinetic energy and turbulent energy dissipation are scaled with the wall shear stress velocity as follows:

$$U^+ = \frac{U}{u_\tau}, \quad k^+ = \frac{k}{u_\tau^2}, \quad \epsilon^+ = \frac{\epsilon\,\nu}{u_\tau^4}. \tag{3.1}$$

The wall shear stress velocity u_τ is calculated with equation 2.17, where the local wall shear stress was obtained from Fluent. The results of the different simulations and literature data are shown in figure 3.4.

Simulations to check grid dependency were done with all grid sizes with inlet conditions A (table 3.3). Simulations to check inlet conditions were done with the standard grid with both inlet conditions. All simulations were done with both types of outlet.

The simulations with the different outlets showed no differences in the end results. There was only a difference in the number of iterations: the 'pressure outlet' converged a little faster than the outflow. For example, the solution was converged after 449 iterations with an 'outflow', while it was converged after 440 iterations with a 'pressure outlet' for the standard grid with inlet conditions A. Nevertheless, the 'outflow' was chosen for simulations with the mixing chambers, because no further specifications need to be given for an outflow and there is only a small difference in the number of iterations.

In figure 3.4 (a) the velocity profile is shown. It can be seen that the solution is dependent on the applied grid. All data are lower than the measured data from [Eggels et al., 1994]. The deviation might be due to the calculation of u_τ, because when velocity is scaled with the centerline velocity (figure 3.4 (b)), the profile matches literature data well. When velocity is scaled with u_τ the coarse grid is nearest to the literature data. When it is scaled with U_{max}, the coarse grid is the worst. The solutions of the other grids are almost the same. The inlet conditions for the axisymmetric, fine, coarse and one standard grid were the inlet conditions A (see table 3.3). The other standard grid was simulated with inlet conditions B (see table 3.4).

The energy dissipation is shown in figure 3.4 (e). The solutions for all grids were the same and comparable to literature. Only near the wall, Fluent had difficulties predicting the energy dissipation. The profiles did not change anymore after $10D$ for both velocity and energy dissipation.

The kinetic energy profiles did change with distance from inlet. This is shown in figures 3.4 (c) and (d). The inlet k^+ is 8.7 for the standard grid with inlet conditions A, 5.1 for the standard grid with inlet conditions B, 5.6 for the fine grid and 10.1 for the coarse grid. After $10D$, the profiles are very different from the profiles found in literature. The profile of the coarse grid develops the slowest, while the fine grid is the fastest and inlet conditions A look better than inlet conditions B. After 30

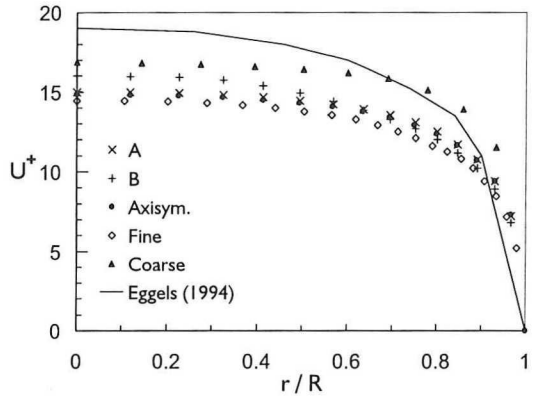

(a) Velocity profile after $10D$.

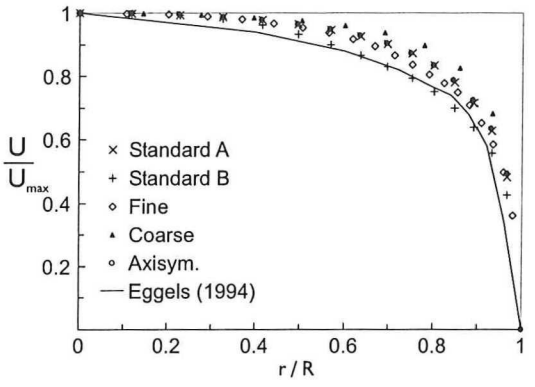

(b) Velocity profile U/U_{max} after $10D$.

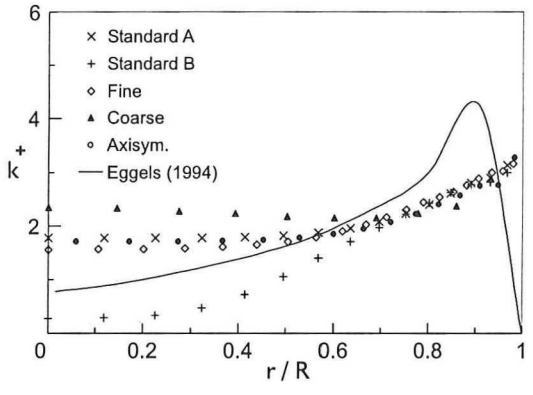

(c) Kinetic energy profile after $10D$.

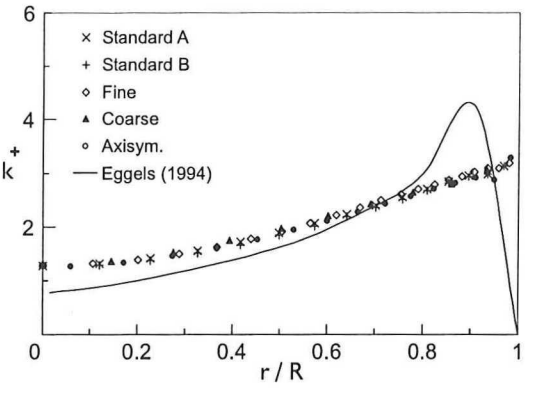

(d) Kinetic energy profile after $35D$.

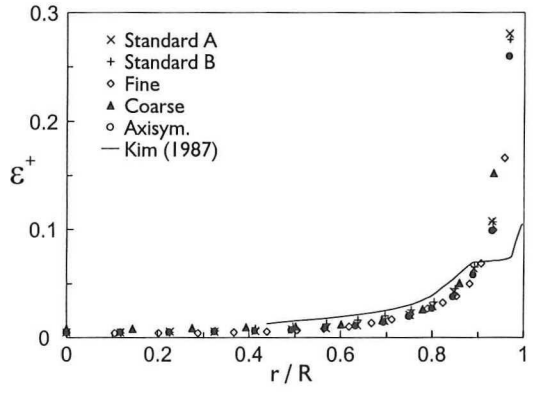

(e) Energy dissipation profile after $10D$.

Figure 3.4: Dependency of turbulent properties of simulation parameters.

diameters, the profiles are the same for all simulations and agree with literature. The most striking difference of the simulations with the data from [Eggels et al., 1994] is the absence of the peak near the wall. In [Hrenya et al., 1995] it is shown that this is a common problem in simulations.

The results show the same fully developed flow for all four grids and for all parameters. The only difference was the developing length for k^+ for the different grids and inlet conditions. The fine grid performed best here. Therefore the grid used for mixer simulations was based on the fine grid. A serious problem is that after $10D$, the kinetic energy does not have a turbulent profile. The inlet conditions used here are not appropriate, so for the mixer, different inlet conditions will be used. These will be discussed in the next section. As the profiles agree with literature, it can be concluded that the used model, the k-ϵ model is appropriate.

3.4 Boundary Conditions, Convergence and Discretization

After the simulations with the pipe, the boundary conditions for the mixer simulations were chosen. These are summarized in table 3.5.

Table 3.5: Boundary conditions for mixer simulations.

Part	Condition
Inlet	Profile for velocity, k and ϵ
Outlet	Outflow
Convergence criteria	10^{-5}
Near-wall simulation	Wall functions
Symmetry plane	Back mixer
Mass fraction A	left inlet: 0.1 right inlet: 0
Mass fraction B	left inlet: 0 right inlet: 0.1

The user defined function (UDF) for the inlet profiles can be found in appendix A. As the mixer outlet has the same diameter as the inlet, Re in the mixer outlet is twice as high as for the inlet (18,000).

3.4.1 Verifying Grid Independency

To be sure of grid independency, different meshes were used, varying from a small to a large number of cells.

3.5 Geometry and Grid

As discussed in paragraph 1.3, two types of mixing chambers were chosen for simulation: a Y-mixer with an angle of 10° and a T-mixer. Because of symmetry, only half of the geometry needed to be simulated. This was shown in figure 2.3.

Both geometries were divided into many cells for simulation. The parameters of these meshes are given in table 3.6. The grids of the cross-sections of the pipes are shown in figure 3.6.

Table 3.6: Grid properties of mixer. (See figures 3.1 and 3.5 for clarification of the letters.)

	T-mixer		Y-mixer	
	Standard	Fine	Standard	Fine
Boundary layer				
- Size first layer (a) [mm]	0.05	0.03	0.05	0.03
- Growth factor (b/a)	1.1	1.05	1.1	1.05
- Number of layers	4	4	4	4
Number of cells				
- Radial (e)	20	22	20	22
◁ Growth factor (d/c)	1.1	1.1	1.1	1.1
- Circumferential (f)	30	40	30	40
- Along j	40	50	40	50
- Along k	20	26	20	26
- Along l	35	45	35	45
- Along m	50	65	50	65
Total number of cells	149,670	265,668	144,400	264,534

All edges in lengthwise direction for all geometries had growth factors (i/h in figure 3.3) in two directions. This means that one half of the volume has a different growth factor than the other half. The halfs that are closest to the center of the geometry have a growth factor of 1.05 (this means a finer mesh towards the center). The other halfs had a growth factor of 1 (all nodes have the same distance).

One pipe was used for comparison. The standard grid described in section 3.3 was used with a length of 35 mm. A and B were injected in a homogeneously mixed solution.

3.6 Particle Tracking

The boundary conditions for particle tracking are as follows. When a particle meets a wall it is 'reflected' (it bounces against the wall) and when it meets an outlet it 'escapes' (the particle has left the computational domain). The Fluent parameters for particle tracking are given in tables 3.7 and 3.8. The material properties of the

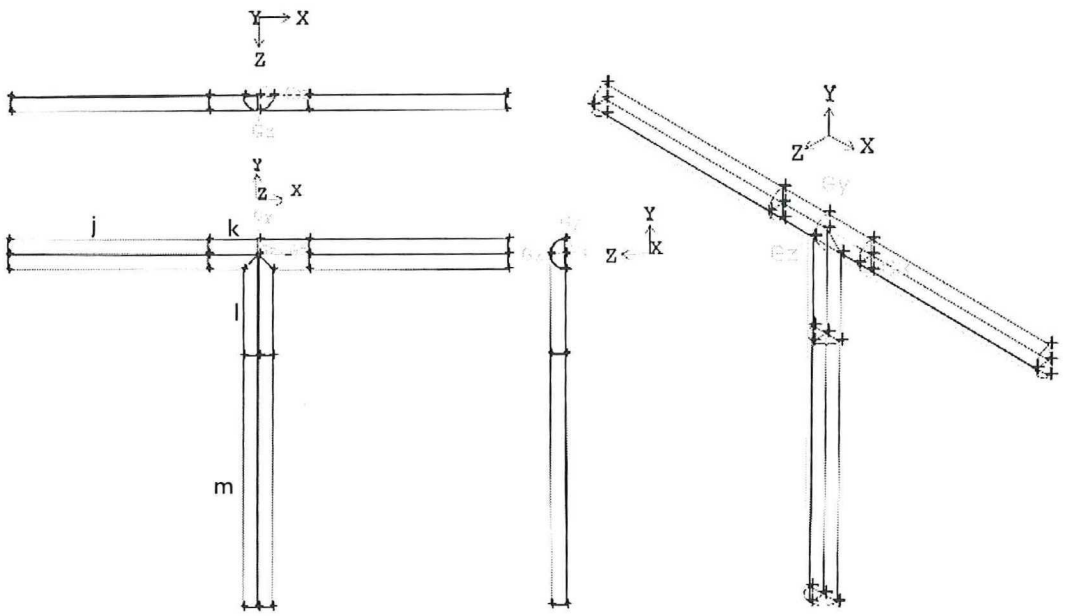

(a) T-mixer

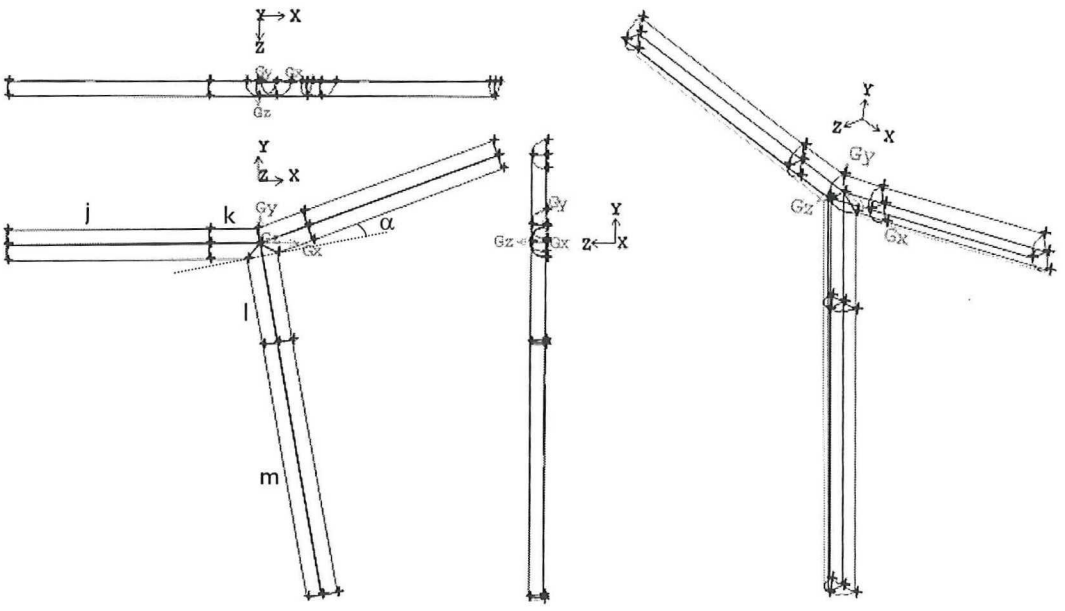

(b) Y-mixer

Figure 3.5: Views of the mixers: bottom, front, side and 3D view.

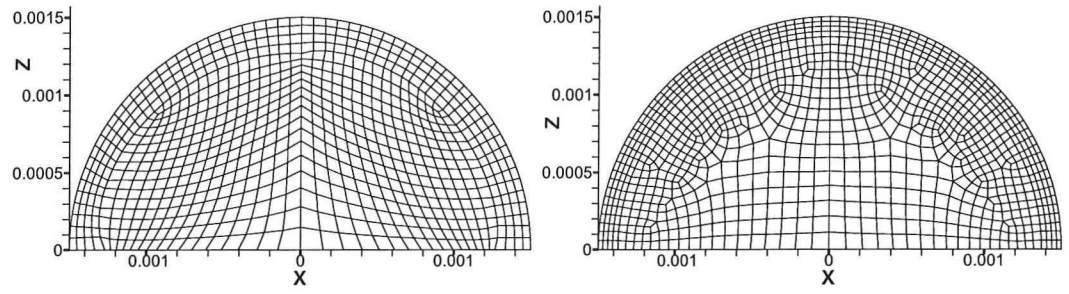

(a) Standard (b) Fine

Figure 3.6: Grid of cross-section of mixer pipes.

particles are the same as water.

Table 3.7: Injection parameters

Number of particles	mixer: 254, pipe: 130
Particle type	inert
Velocity	0 (in all directions)
Diameter	10^{-6}
Temperature	300 K
Mass-flow	0

Table 3.8: Tracking parameters

Max. number of steps	7000
Length scale	0.0001 m
Drag law	spherical
Interaction with continuous phase	none

The particles were injected in a circular manner, starting from the origin of the semi-circle. This is shown in figure 3.7.

Mixing is only important from the moment the different species 'see' each other. Therefore the following steps are done for the mixed region only, where $m_A \times m_B$ is not equal to 0. A boundary of $m_A \times m_B \geq 10^{-8}$ was chosen. Of the particle trajectories after this point the history of energy dissipation will be obtained. The energy dissipation will be used to calculate the time for micromixing of species A and B. From the energy dissipation, a characteristic micromixing time can be calculated. Each particle has an energy dissipation history from which a time scale history can be calculated. The energy dissipation will be integrated per particle.

$$\bar{\epsilon} = \frac{\sum_0^{t_r} \epsilon \Delta t}{t_r} \tag{3.2}$$

where t_r is the residence time of the particle over the selected trajectory, ϵ the energy dissipation over the length with time step Δt and ϵ the average energy dissipation

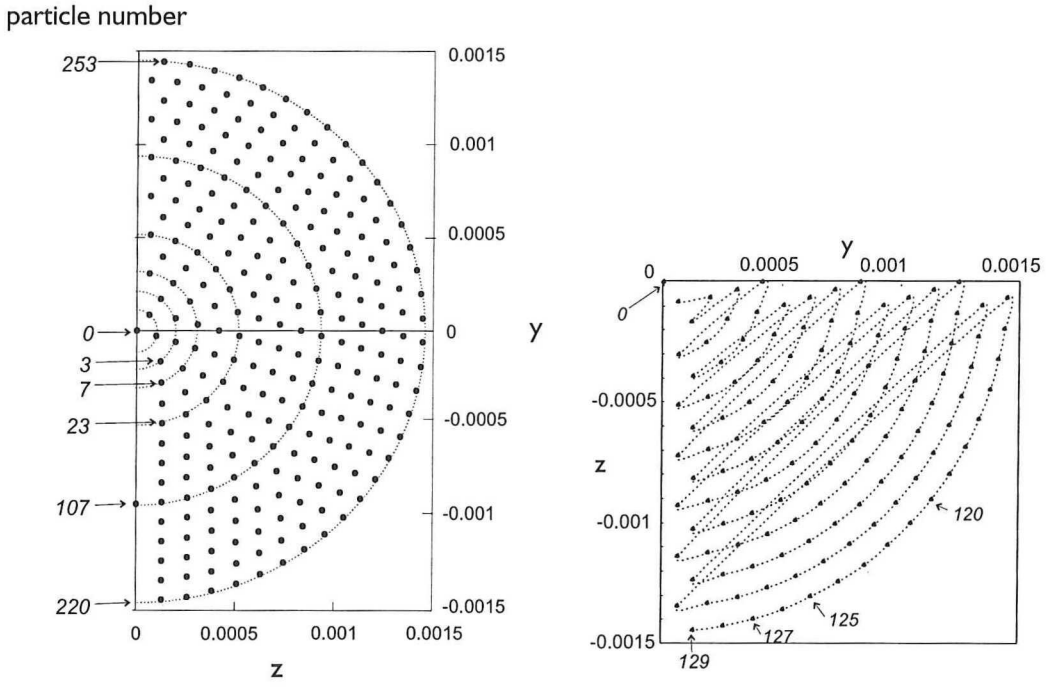

(a) Mixer (b) Pipe

Figure 3.7: Coordinates of particle injections and particle numbers. The dotted line shows the order of the particle numbers.

over the particle trajectory. The Matlab code for these calculations can be found in appendix B.

Chapter 4

Results and Discussion

4.1 Velocity Vectors

From the simulations in Fluent, the following properties were considered: velocity profile, kinetic energy, energy dissipation and mass fraction of species A.

The velocity vectors on the symmetry plane of the center of the T- and Y-mixers are shown in appendix C, figures C.1 and C.2. In these plots each vector indicates the direction and the length and color indicate the magnitude of the velocity in a cell. Not all vectors are shown, because of clarity. In figure C.1 (a) it can be seen that the fine mesh is asymetric, but this has no influence on the results. It looks like there are less cells on the left side of the mixer, but this is not the case, the vectors of the cells in between are not shown. For both T- and Y-mixers, the fluid on the top of the mixer is hardly moving. This might be due to the lack of space where the fluid can go. The fluid wants to go straight, but then it impinges with the other stream. In the Y-mixer, the fluid has more momentum towards the outlet, but this seems to have little influence on this zone. There is a little bit of backmixing just downstream the corners. The flows in the T- and Y-mixers are similar.

4.2 Contour Plots

The profiles of kinetic energy, energy dissipation and mass fraction on the T- and Y-mixer symmetry planes are shown in appendix C, figures C.3, C.4, C.5, C.6, C.7 and C.8. If the results are the same for the standard grid compared to the fine grid, the results are independent of grid size. In this section, the profiles of the symmetry planes were compared visually.

Comparison grids of T-mixer
The kinetic energy graphs are shown in figure C.3. The results are similar, except the

slightly higher kinetic energy near the wall in the fine mesh. The energy dissipation profiles (figure C.5) do not show any differences. In the species profiles (figure C.7), the species are mixed a little bit earlier for the fine grid. For all properties, the profiles look very much the same for both grid sizes.

Comparison grids of Y-mixer
The kinetic energy (figure C.4) of the fine grid is a little higher than the kinetic energy in the standard grid. Furthermore, shortly downstream the corners the kinetic energy is a little bit higher in the fine mesh. For the energy dissipation (figure C.6) and mass fraction of A (figure C.8) there are no big differences.

Comparison T- and Y-mixer
The kinetic energy has the largest difference between the geometries. Turbulent energy dissipation is high until four pipe diameters from impingement point for both mixers. In the T-mixer, the kinetic energy is larger in the center than in the Y-mixer. The energy dissipation shows a difference as well. The energy dissipation in the center and just downstream the edges is larger for a T-mixer. In the mass fraction profiles it can be seen that the T-mixer mixes faster than a Y-mixer, because the green part (A and B having equal mass fractions) at the outlet is larger.

4.3 Mixing Chamber Characterization

One particle follows a certain trajectory and encounters different levels of energy dissipation (figure 4.1) and concentrations of reactants (figure 4.2). As mixing is only important when the two species get into contact with each other, the data are filtered on species concentration. The starting conditions are defined as $m_A \times m_B \geq 10^{-8}$. The end point can be defined on different places in the outlet tube. Here it was the outlet plane of the outlet pipe. In figure 4.2, the mass fractions of A and B are shown and in figure 4.3 an example of the energy dissipation levels. Both figures show the variables encountered by particle 253. In the figures, the dotted part of the lines show the whole trajectory, the solid lines show the data used in the calculations.

In the ideal case, mass fraction of A and the mass fraction of B are mixed completely, which means $m_A = m_B = 0.5$. For the particle in figure 4.2 this is not achieved and this is valid for most of the particles as can be seen in figures C.7 and C.8, where only the center shows $m_A = m_B = 0.5$. The outlet of the mixer is too short for complete mixing of A and B.

4.4 Time Scale Calculations

Different time scales were discussed in paragraph 2.6. A quick analysis gives the following magnitudes for these time scales for an energy dissipation of 1000 m^2s^{-3} (see table 4.1).

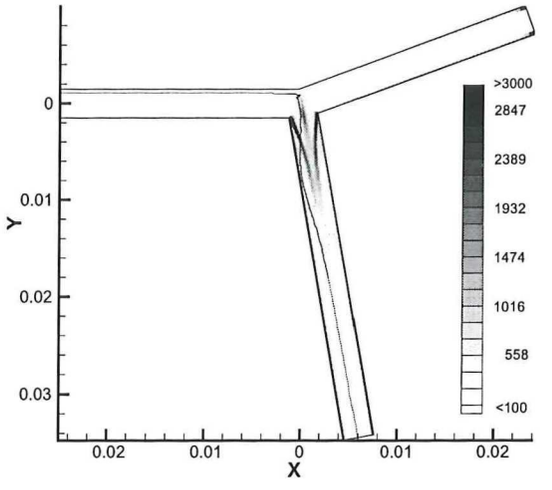

Figure 4.1: Energy dissipation in symmetry plane of Y-mixer, with path of a particle. (particle 253 of Y-mixer)

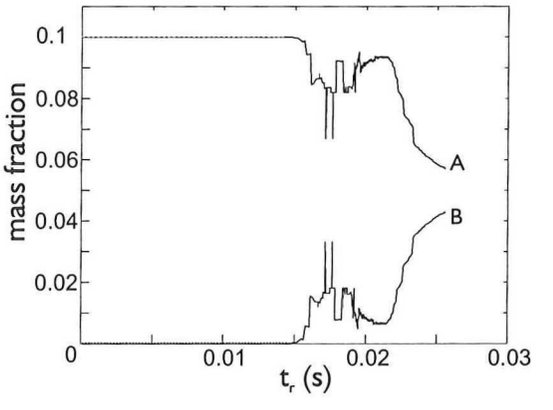

Figure 4.2: Mass fraction vs residence time of particle. The upper line is the mass fraction of A, the lower line that of B. (particle 253 of Y-mixer)

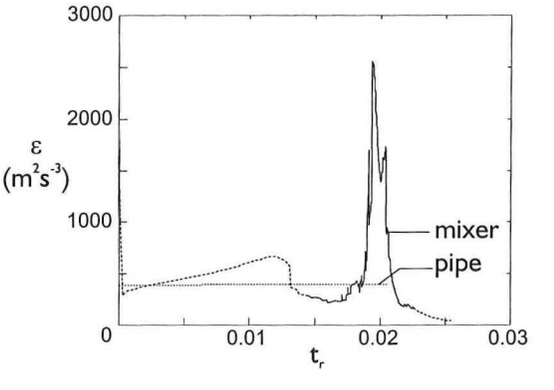

Figure 4.3: Energy dissipation encountered by one particle in a mixer (particle 253 of Y-mixer) and pipe.

Table 4.1: Different time scales

Time scale Author(s)	Order of magnitude of mixing time (ms)
Micromixing time Demyanovich and Bourne (1989)	8
Micromixing time Geisler et al. (1988)	12
Homogenization time Corrsin (1964)	1.1
Engulfment time Shekunov et al. (2001)	0.5

The first two scales are in the same order of magnitude. Both times are micromixing times, based on diffusion over the Kolmogorov length scale and are dependent of Sc and ν/ϵ. The time scales gives the time it takes for diffusion over the length scale. The Corrsin time scale is ten times smaller. It consists of two parts, $\frac{3}{2}k/\epsilon$ and ν/ϵ. $\frac{3}{2}k/\epsilon$ gives the time for turbulence decay. For the conditions in the mixer, this term is about 30 times larger than the diffusion term. This time appears in an exponential factor and does therefore not give a time for completion of mixing, but it looks more like a half life; the rate at which the concentration difference decreases. The engulfment time is again smaller. It is based on the theory of engulfment of small eddies, which is the last stage of a series of energy dissipating eddies. For analysis two time scales were chosen, one based on diffusion: [Demyanovich and Bourne, 1989] and one based on engulfment time: [Bałdyga and Bourne, 2000]. The first time was chosen, because it is straightforward and it describes a simple process. The second is chosen, because it is based on a different kind of homegenization, namely the decay of the smallest eddy. This is not a diffusion process.

4.5 Time Scale Plots

The following plots were made with a particle step size of 10^{-3} m and with 10^{-4} m. The plots with these step sizes were not significantly different, therefore only the plots with a step size of 10^{-4} m are shown. In the time scale plots each dot represents one particle.

4.5.1 Residence Time Distribution

In figure 4.4 the residence times of the mixers are given. They are plotted against particle number. The location of injection of each particle can be found in figure 3.7. For each grid, two residence times are shown. One is the residence time of the particle in the complete mixer ($\diamond$). The total length of the mixer (along centerlines

of each pipe) is 25 + 35 mm, corresponding to $20D$. The second (*) is the residence time from the point where $A \times B \geq 10^{-8}$ to the end of the mixer, but the length of the track covered by a particle differs for each particle, because the starting point for each particle is different and because of the bend in the trajectory.

First it must be noted that the flow looks like plug flow in the 3D particle trajectory pictures. These are not shown here, because of the complexity of the 3D picture. In turbulent flows there usually is no plug flow, because of the velocity fluctuations. In this study, the particles are following the average flow instead of the turbulent velocity field, so there is plug flow in these results.

The figure shows that the residence time increases when the particle number gets larger. As can be seen in figure 3.7, a larger particle number means that the particle is injected nearer to the wall of the inlet. This corresponds to the notion that the velocity decreases nearer to the wall. Another feature is the oscillating pattern of the residence time. It shows that particles injected at the bottom part of the inlet are faster than those injected at the top part. This might be due to the shorter trajectory they have to travel, because of the curve in the trajectory. The starting point criterion may also be of influence here (see appendix C, figures C.7 and C.8). There are no big differences between the T- and Y-mixer.

4.5.2 Micromixing Time

In figure 4.5 a plot of micromixing time vs residence time from $A \times B \geq 10^{-8}$ to the outlet of the mixer is given. The micromixing time was calculated according to equation 3.2. The Matlab file used for calculation is given in appendix B. It shows the relation between the time needed for mixing on microscale and the time a particle (part of the fluid) is allowed to mix to molecular scale. If the micromixing time is equal to or lower than residence time, mixing of the two reactants is completed. The sloped line shows $t_m = t_r$. Particles below this line are micromixed homogeneously, while particles above this line have not yet completed micromixing at the mixer exit.

As can be seen in the figures, micromixing times are much larger than residence times. Micromixing is not fast enough. Most of the particles have a micromixing time around 0.02 s, but the fluid has not enough time to mix completely. The relation between location of injection and mixing times is as follows. The particles injected in the center of the inlet have a large t_m (larger than 0.02 ms). The nearer injected to the wall, the smaller t_m, because near the wall, the energy dissipation is higher (see figures C.5 and C.6). The particles injected in the top near the wall are recognizable by their long t_r and most of these particles are below the $(t_m = t_r)$-line. Again, there are no significant differences between a T-mixer and a Y-mixer.

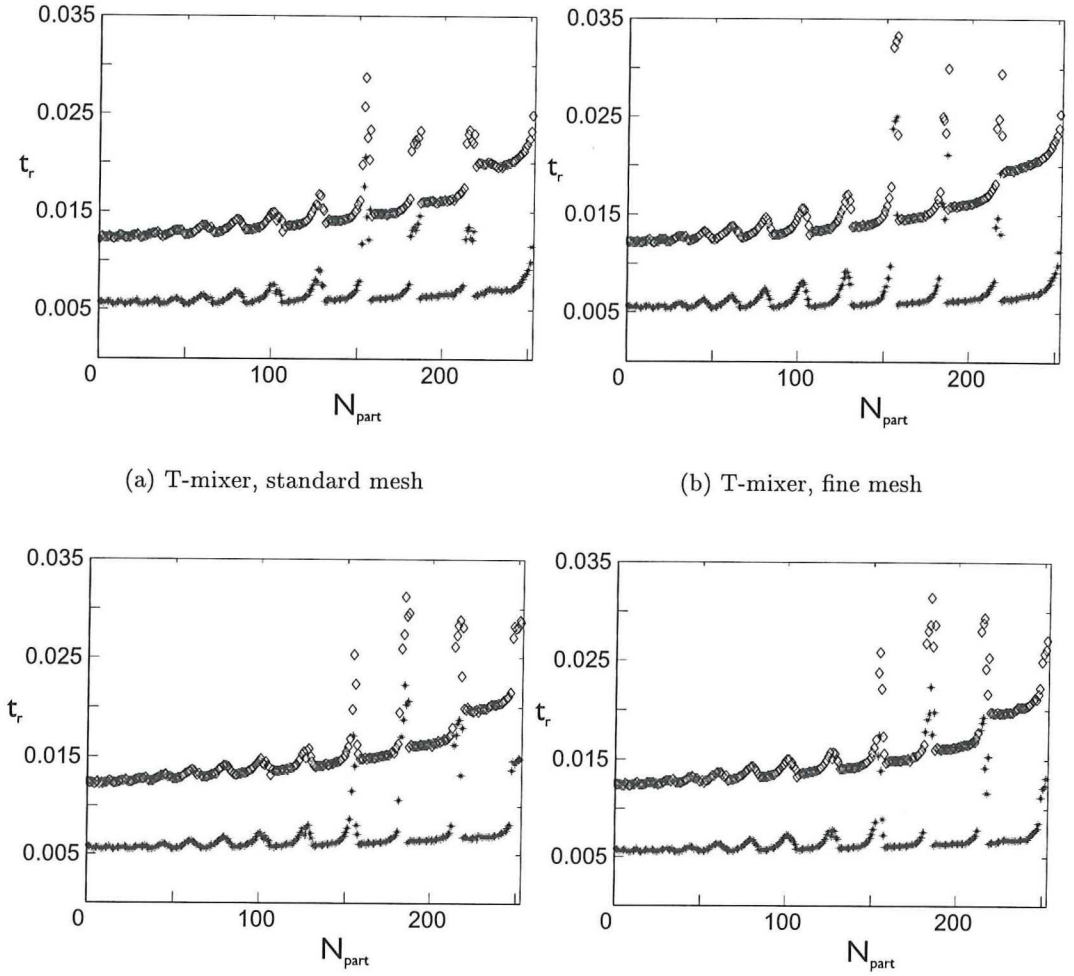

(a) T-mixer, standard mesh

(b) T-mixer, fine mesh

(c) Y-mixer, standard mesh

(d) Y-mixer, fine mesh

Figure 4.4: Residence time distribution of whole mixer (◇) and of selected part (*)

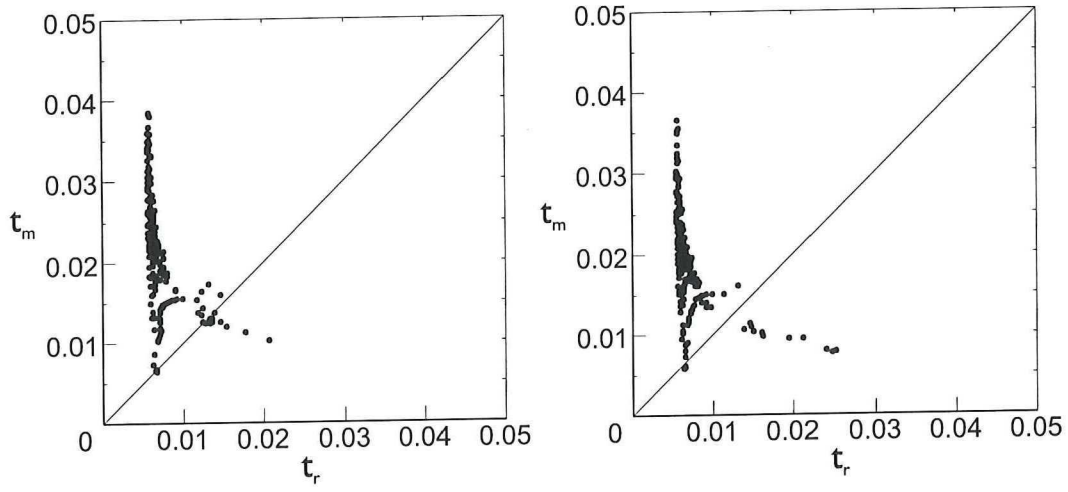

(a) T-mixer, standard mesh

(b) T-mixer, fine mesh

(c) Y-mixer, standard mesh

(d) Y-mixer, fine mesh

Figure 4.5: Micromixing time.

4.5.3 Engulfment Time

The engulfment time scale plots are shown in figure 4.6. For all particles, the engulfment time is smaller than the residence time, so the process of engulfment is completed at the outlet of the mixer. The plots have the same shape as the micromixing time plots, because both depend on $\epsilon^{-1/2}$, see equations 2.57 and 2.59. The engulfment time is shorter, because the factor in front of $\epsilon^{-1/2}$ ($17.24\nu^{1/2}$) is 15 times smaller than the constant in micromixing time ($0.25 \cdot Sc \cdot \nu^{1/2}$, with $Sc = 1000$ and $\nu = 10^{-6}$ m^2s^{-1}). The time is smaller because a different process is described. The process of diffusion over the Kolmogorov length is slower than the decay of an eddy.

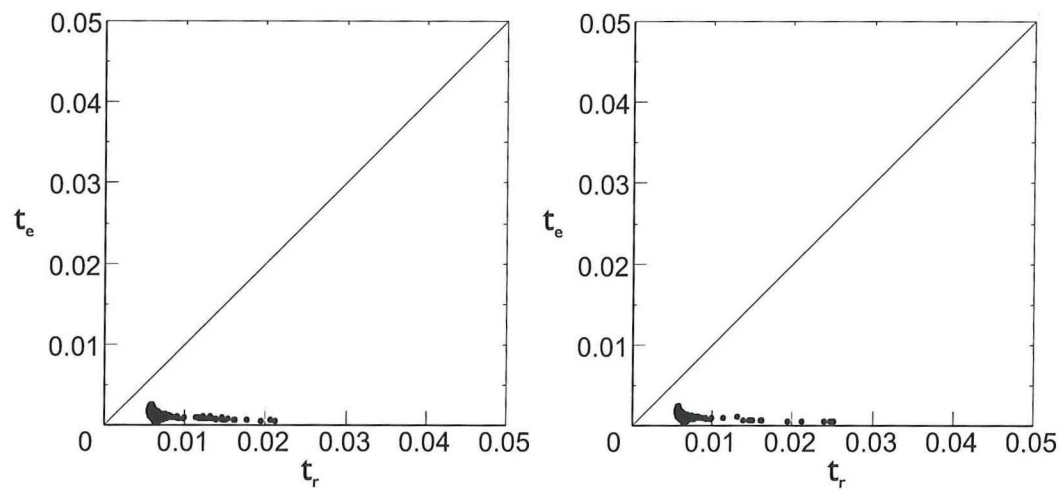

(a) T-mixer, standard mesh

(b) T-mixer, fine mesh

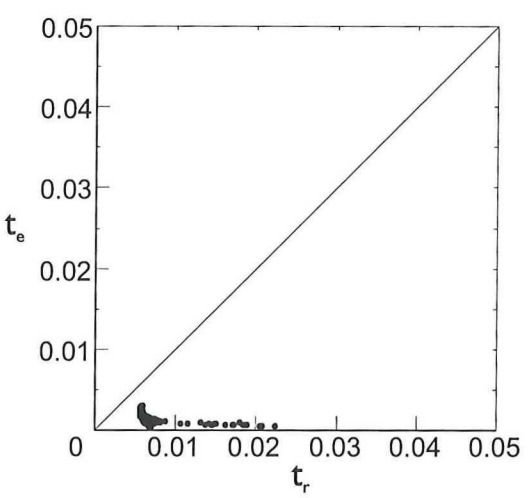

(c) Y-mixer, standard mesh

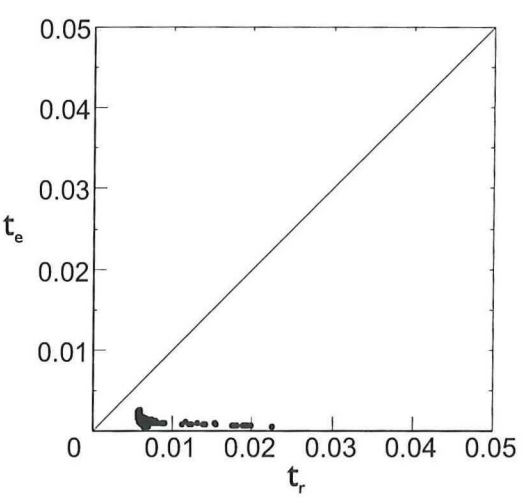

(d) Y-mixer, fine mesh

Figure 4.6: Engulfment time.

4.5.4 Comparison with Pipe Flow

For comparison, the results of a pipe, described in paragraph 3.3, with the same turbulent inlet conditions as the mixers and a length of 35 mm ($11\frac{2}{3}D$)are shown in figure 4.7. The profiles of kinetic energy and energy dissipation are shown in figure C.9. When comparing this pipe with the results of the mixer, caution has to be taken, because *Re* in the pipe is 9,000, while it is 18,000 in the outlet of the mixer. Also, the part of the pipe simulated was a quarter, instead of a half pipe, like for the T- and Y-mixer. This is the reason why there are less particles injected compared to the T- and Y-mixer. The pattern of injection was the same. (See figure 3.7).

The residence time distribution does not show an oscillating pattern as in the T- and Y-mixer, because it is a straight pipe; there are no effects of a bend in the flow. Secondly, the calculations start at the inlet of the pipe and finish at the outlet, because there was a homogeneous mixture of A and B injected at the inlet, so the start criterion was already fulfilled.

It is clear that micromixing times in the pipe are much larger than micromixing times in a T- or Y-mixer. When *Re* is twice as high as it was in this simulation, it is not expected that the micromixing time will be lower, because the energy dissipation in the center of the pipe stays low.
For pipe flow, the engulfment time is also smaller than the residence time.

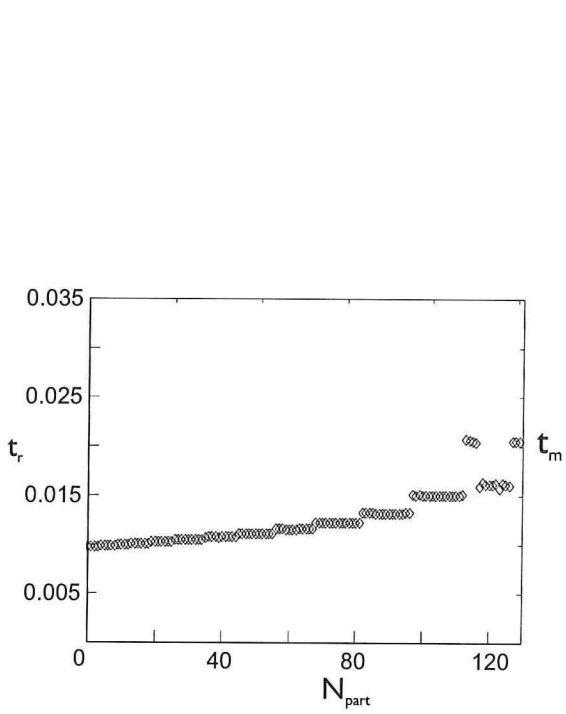

(a) Residence time distribution

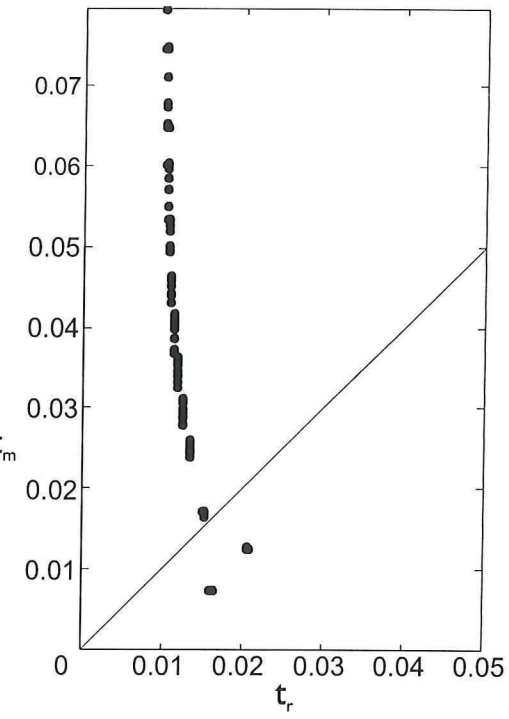

(b) Micromixing time

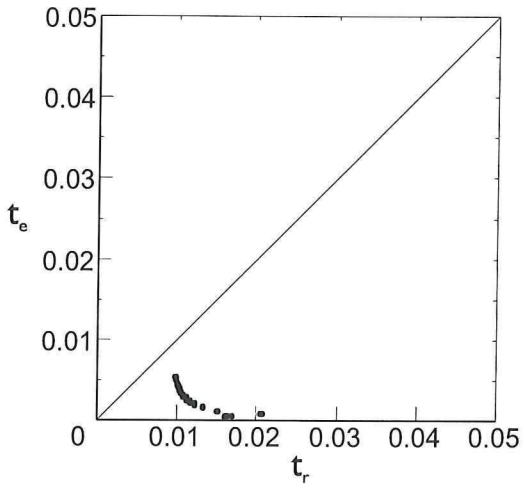

(c) Engulfment time

Figure 4.7: Pipeflow results.

Chapter 5

Conclusions and Recommendations

In this thesis, two mixing chambers were studied, a Y-mixer and a T-mixer. The mixing performances of these two mixers were compared with the help of the CFD package Fluent 6.0.20.

5.1 Conclusions

The following properties were compared on the symmetry plane of the mixers. The velocity profiles and mass fraction profiles of the T- and Y-mixer and the profiles for kinetic energy and energy dissipation of the T-mixer, Y-mixer and pipe were compared. The velocity profiles for the T- and Y-mixer show a small region of non-moving fluid on the top of the mixing region. Just downstream the edges, there was a little bit of backmixing. The flow in the T- and Y-mixer is similar, in spite of the different shape.
From the mass fraction profiles can be concluded that macromixing is not complete. The two species have not mixed completely at the end of the outlet. Only in the center both species have mixed. The macromixing in the T-mixer looks slightly better.
The profiles for kinetic energy and energy dissipation show a high kinetic energy and high energy dissipation in the impingement zone, up to four diameters of the start of the outlet pipe. The levels were much higher than those in the pipe. In a T-mixer the kinetic energy in the beginning of the outlet pipe was higher.
The profiles for the different grids showed no significant differences, therefore it can be concluded that the solution was independent of the applied grid.

The residence time distribution shows that plugflow is present in the mixers and pipe when particles are following the average flow.

In the CFD package Fluent 6.0.20 only the macromixing is calculated. Because reaction takes place at smaller scales, micromixing times were also considered. The T- and Y-mixers were characterized with help of mixing times: micromixing time t_m and engulfment time t_e. These times describe different processes. The micromixing time is based on diffusion over the Kolmogorov length, while the engulfment time gives the time for decay of the smallest eddy. These times were obtained with help of particle tracking. With particle tracking, the history of energy dissipation was obtained from the point where A $\times$ B $\geq 10^{-8}$. The energy dissipation was averaged per particle and from this value the mixing times were calculated. The characteristic times were summarized in a (t_m, t_r) and (t_e, t_r)-plot, i.e. micromixing was plotted versus residence time and in another plot, the same with engulfment time. The plots have the same shape, but the engulfment time is 15 times smaller than the micromixing times. The fact that the micromixing times are larger than the residence time means that a fluid element has not sufficient time to mix completely during the time in the mixer. The engulfment process appears to be completed at the outlet of the mixer.

The mixers are not suitable for fast mixing, on macroscale as well as on microscale and there are no significant differences between a T- and a Y-mixer.

5.2 Recommendations

The results show that the micromixing time is not short enough for the precipitation experiments. Therefore it is better not to use just a T- or a Y-shaped mixing chamber for mixing. To ensure better mixing with the current T- or Y-mixer, an additional static mixer might be used downstream of the mixer.

The mixing times selected in this thesis were based on diffusion over Kolmogorov scale and on engulfment, which is the last stage in a series of events. Another event might be the limiting step i.e. take a longer time to complete. It is best to characterize a mixing chamber on the limiting characteristic time, which might not be the characteristic time chosen in this thesis.

The micromixing time was compared to residence time. It is also possible to compare with the nucleation time (time before small particles start to form) of the precipitate. If the micromixing time is faster than nucleation time, the crystals precipitate in a homogeneously mixed solution. This is only possible when macromixing is good, otherwise there are large parts of the fluid that are not mixed at all.

An option to increase mixing performance might be a higher velocity as far as this is not limited by pressure drop. A higher velocity means a higher *Re* and faster moving fluids impinging onto each other, which causes the higher kinetic energy and energy dissipation.

A different geometry might be used for mixing. Possibly a mixer with more than

two inlets or a vortex mixer.

To validate these CFD results, precipitation or mixing experiments might be performed.

Appendix A

UDF for Inlet Profile

```
/************************************************************************
 * UDF for specifying fully-developed profile boundary conditions       *
 * voor een HALVE buis (zowel T als Y menger)                           *
 ************************************************************************/

#include "udf.h"

/* constants  */

#define YMIN -0.0015          /* voor T */
#define YMAX 0.0015
#define YMINS 0.007141        /* voor Y */
#define YMAXS 0.009960
#define RADIUS 0.0015
#define XC 0.0234923          /* x-coord. center inlet-scheef */
#define YC 0.0085505          /* y-coord. center inlet-scheef */
#define UMEAN 3.0             /* gem. snelheid */
#define B 1./6.               /* exponent velocity profile */
#define VISC 1e-06            /* viscositeit (nu) water */
#define CMU 0.09
#define VKC 0.41


/*  profile for x-velocity RECHT   */

DEFINE_PROFILE(v_r_profile, thread, position)
{
  real y, z, r, del, h, x[ND_ND], ufree;         /* variable declarations */
  face_t f;

  ufree = UMEAN*(B+1.);

  begin_f_loop(f, thread)
    {
      F_CENTROID(x,f,thread);
      y = x[1];
      z = x[2];
      r = sqrt(y*y + z*z);

      F_PROFILE(f,thread,position) = ufree*pow(1-(r/RADIUS),B);
    }
  end_f_loop(f, thread)
}


/* Velocity SCHEEF */

DEFINE_PROFILE(v_s_profile, thread, position)
{
  real q, y, z, r, x[ND_ND], ufree;         /* variable declarations */
  face_t f;

  ufree = UMEAN*(B+1.);

  begin_f_loop(f, thread)
    {
      F_CENTROID(x,f,thread);
```

```
      q = x[0]-XC;
      y = x[1]-YC;
      z = x[2];
      r = sqrt(q*q + y*y + z*z);

      F_PROFILE(f,thread,position) = ufree*pow(1-(r/RADIUS),B);
    }
  end_f_loop(f, thread)
}


/*  profile for kinetic energy RECHT  */

DEFINE_PROFILE(k_r_profile, thread, position)
{
  real y, z, r, del, ufree, x[ND_ND];
  real ff, utau, knw, kinf;
  face_t f;

  ufree = UMEAN*(B+1.);
  ff = 0.045/pow(ufree*RADIUS/VISC,0.25);
  utau=sqrt(ff*pow(ufree,2.)/2.0);
  knw=pow(utau,2.)/sqrt(CMU);
  kinf=0.002*pow(ufree,2.);


  begin_f_loop(f, thread)
    {
      F_CENTROID(x,f,thread);
      y = x[1];
      z = x[2];
      r = sqrt(y*y + z*z);

      F_PROFILE(f,thread,position)=knw+(1-(r/RADIUS))*(kinf-knw);
    }
  end_f_loop(f, thread)
}


/*  profile for kinetic energy SCHEEF  */

DEFINE_PROFILE(k_s_profile, thread, position)
{
  real q, y, z, r, ufree, x[ND_ND];
  real ff, utau, knw, kinf;
  face_t f;

  ufree = UMEAN*(B+1.);
  ff = 0.045/pow(ufree*RADIUS/VISC,0.25);
  utau=sqrt(ff*pow(ufree,2.)/2.0);
  knw=pow(utau,2.)/sqrt(CMU); /* near wall value */
  kinf=0.002*pow(ufree,2.);         /* free stream value */


  begin_f_loop(f, thread)
    {
      F_CENTROID(x,f,thread);
```

```
      q = x[0]-XC;
      y = x[1]-YC;
      z = x[2];
      r = sqrt(q*q + y*y + z*z);

      F_PROFILE(f,thread,position)=knw+(1-(r/RADIUS))*(kinf-knw);
    }
  end_f_loop(f, thread)
}


/* profile for dissipation rate RECHT */

DEFINE_PROFILE(e_r_profile, thread, position)
{
  real y, z, r, x[ND_ND], del, h, ufree;
  real ff, utau, knw, kinf;
  real mix, kay;
  face_t f;

  ufree = UMEAN*(B+1.);
  ff = 0.045/pow(ufree*RADIUS/VISC,0.25);
  utau=sqrt(ff*pow(ufree,2.)/2.0);
  knw=pow(utau,2.)/sqrt(CMU);
  kinf=0.002*pow(ufree,2.);

  begin_f_loop(f, thread)
    {
      F_CENTROID(x,f,thread);
      y = x[1];
      z = x[2];
      r = sqrt(y*y + z*z);

      kay=knw+(1-r/RADIUS)*(kinf-knw);

      if (VKC*(RADIUS-r) < 0.085*RADIUS)
        mix = VKC*(RADIUS-r);
      else
        mix = 0.085*RADIUS;

      F_PROFILE(f,thread,position)=pow(CMU,0.75)*pow(kay,1.5)/mix;
    }
  end_f_loop(f,thread)
}


/* profile for dissipation rate SCHEEF */


DEFINE_PROFILE(e_s_profile, thread, position)
{
  real q, y, z, r, x[ND_ND], del, h, ufree;
  real ff, utau, knw, kinf;
  real mix, kay;
  face_t f;

  ufree = UMEAN*(B+1.);
```

```
  ff = 0.045/pow(ufree*RADIUS/VISC,0.25);
  utau=sqrt(ff*pow(ufree,2.)/2.0);
  knw=pow(utau,2.)/sqrt(CMU); /* near wall value */
  kinf=0.002*pow(ufree,2.);          /* free stream value */

  begin_f_loop(f, thread)
    {
      F_CENTROID(x,f,thread);
      q = x[0]-XC;
      y = x[1]-YC;
      z = x[2];
      r = sqrt(q*q + y*y + z*z);

      kay=knw+(1-r/RADIUS)*(kinf-knw);     /* kinetic energy */

      if (VKC*(RADIUS-r) < 0.085*RADIUS)
        mix = VKC*(RADIUS*r);
      else
        mix = 0.085*RADIUS;

      F_PROFILE(f,thread,position)=pow(CMU,0.75)*pow(kay,1.5)/mix;
    }
  end_f_loop(f,thread)
}
```

Appendix B

Matlab File For Mixing Times Calculation

```
%*********************************************************%
%                                                         %
% P A R T I C L E   T R A C K   C A L C U L A T I O N S   %
%                                                         %
%*********************************************************

clear all;          % Remove all variables from workspace
format short e;

%%%  ====================================================
%%%  DEFINE CONDITIONS
%%%  ====================================================
min_particle_no = 0;
max_particle_no = 253;
%%%  ----------------------------------------------------
%geometry=2; %%% Y

%file = 'Case-yscheef-finer/fine70-';
%file = 'Case-y-scheef/y-circ70-';
%%%  ----------------------------------------------------
geometry=1;    %%% T

%file = 'Case-t-finer/fine70-';
file = 'Case-t34-tcirc70/tcirc70-';
%%%  ----------------------------------------------------
%%%  Filter on concentration in the beginning?
do=1;            %%% Yes
%do=0;       %%% No
%%%  ----------------------------------------------------
%%%  Filter at the end at how many D?
%%%             1 <= D <= 12 (outlet)
dist=4;
%%%  ====================================================


% Constants
% =====================
D = 1e-9;        % Diffusion coefficient (m2/s)
nu = 1e-6;          % Kinematic viscosity (m2/s)
alpha = 1/18*pi; % Angle between inlet and outlet (=10o)
R = 0.0015;         % Radius of pipes of mixer (m)

% Read the file (binary)
% =====================
for particle_no = min_particle_no:max_particle_no
   [number, errmsg] = sprintf('%i',particle_no);
   filename = [file , number]
   fidread = fopen(filename,'r');

   % If file was not opened successfully, fid = -1
   if fidread == -1
      disp('ERROR: File could not be opened!')
   else

      % Read formatted data from file in matrix A
      % =================================================
      % originally 10 columns, become rows in Matlab
      % 1:x, 2:y, 3:z, 4:u, 5:v, 6:w,
      % 7:t, 8:dis. rate, 9:w_A, 10:w_B
      alldata=fscanf(fidread,'%g %g %g %g %g %g %g %g %g %g',[10, inf]);
      fclose(fidread);
      [row, column] = size(alldata);

      % ------------------------ Start concentration filter
      if do==1
         % Select on presence of A and B
         % If mf_A x mf_B < 1e-8 data will not be used
         % ============================================

         clear AxB k i matrix2 column2
         k=0;
         for i = 1:column
            AxB = alldata(9,i)*alldata(10,i);
            if AxB >= 1e-8
               k=k+1;
               matrix2(:,k) = alldata(:,i);
            end

            %       Matrix2 starts at the position
            %       where A and B are both present.
         end
         [row,column2]=size(matrix2);

      else
         matrix2=alldata;
         %       If there is not filtered on presence of A
         %       and B the matrix has the same name for
         %       further calculations.
      end
      % ------------------------ End concentration filter
```

```
    % -------------------------- Start end filter
    clear plane matrix3 column3 plane yfx

    % for a T-mixer
    if geometry==1
       plane = dist*-0.003; % y-coordinate endplane

       for i=1:column2
          if matrix2(2,i) >= plane
             matrix3(:,i) = matrix2(:,i);
          end
       end

       % for a Y-mixer
    elseif geometry==2
       for i=1:column2
          % The end plane had the following
          % formula
          plane=dist*0.003;
          yfx=tan(alpha)*matrix2(1,i)-plane/cos(alpha);

          if matrix2(2,i) >= yfx;
             matrix3(:,i) = matrix2(:,i);
          end
       end

    else
       % If there is no T or Y selected:
       matrix3=matrix2;
       disp('!!!--- no geometry selected ---!!!')
    end

    [row,column3]=size(matrix3);
    % ---------------------------- End end filter


    %---------- Start calculations (per particle)
    clear tm te dt average_m average_e restime

    % Mixing times
    % ===============
    for i = 1:column3
       % Micromixing time
       tm(i,1) = (0.25/D)*sqrt(nu^3/matrix3(8,i));
       % Engulfment time
       te(i,1) = 17.24*sqrt(nu/matrix3(8,i));
       % Period of time
       if i==1
          dt(1,i) = matrix3(7,i);
       else
          dt(1,i) = matrix3(7,i) - matrix3(7,i-1);
       end
    end
 end


 % Average mixing time for one particle
 % ======================================

 % Micromixing time
 average_m = sum(dt.*tm')/sum(dt);
 averageall_m(particle_no+1,1) = average_m;
 % Engulfment time
 average_e = sum(dt.*te')/sum(dt);
 averageall_e(particle_no+1,1) = average_e;


 % Residence time of all particles in one matrix
 % ================================================
 partno(particle_no+1,1) = particle_no;
 % Whole mixer
 taum(particle_no+1,1) = alldata(7,column);
 % Filtered data
 restime = matrix3(7,column3)-matrix3(7,1);
 tr_p(1,particle_no+1) = restime;
 % --------------- End calculations (per particle)
end
```

```
% ------------------------------------- Start figures
n=0;

% Residence time distribution
% ============================
n=n+1;
figure(n)
if dist == 12
plot(partno(:,1),taum(:,1),'kd',partno(:,1),tr_p(:,1),'k*')

else
   plot(partno(:,1),tr_p(1,:),'k^')
end
axis([0 max_particle_no+1 0 0.035])
xlabel('N_{part}')
ylabel('t_{r}')

% Micromixing time vs residence time
% ===================================
n=n+1;
figure(n)
x=0:0.01:0.05;
plot(tr_p(1,:),averageall_m(:,1),'k.',x,x,'k-')
axis image
xlabel('t_r')
ylabel('t_m')

% Engulfment time vs residence time
% ===================================
n=n+1;
figure(n)
x=0:0.01:0.05;
plot(tr_p(1,:),averageall_e(:,1),'k.',x,x,'k-')
axis image
xlabel('t_r')
ylabel('t_e')
% ------------------------------------- End figures
```

Appendix C

Fluent Output

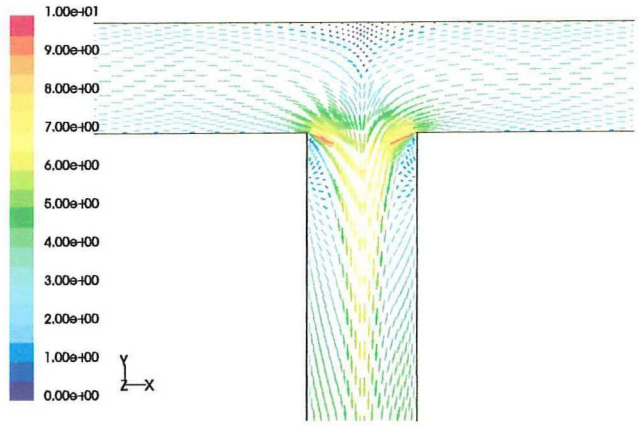

(a) Standard

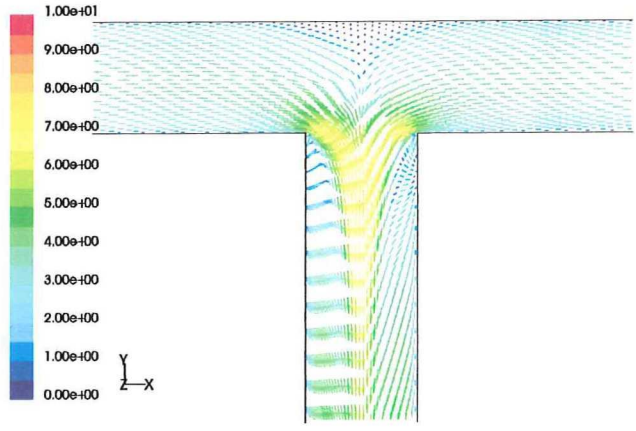

(b) Fine

Figure C.1: Velocity vectors in T-mixer, each vector indicates the velocity in a cell, but not all vectors are shown.

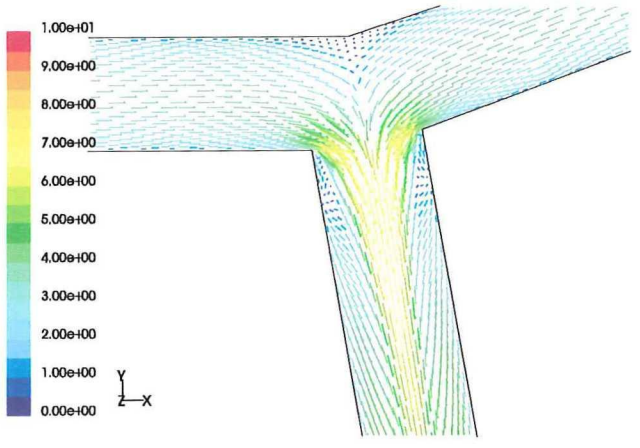

(a) Standard

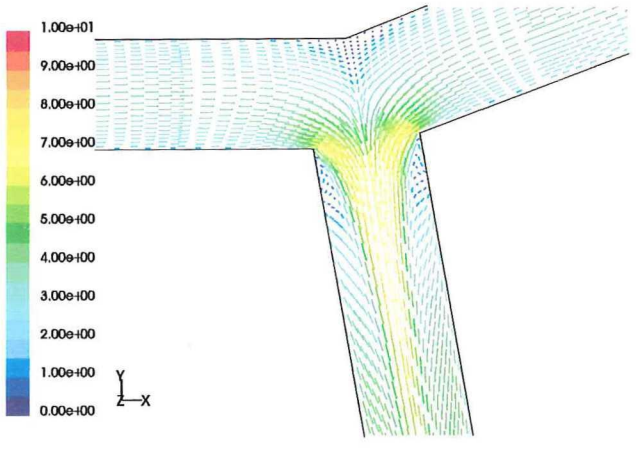

(b) Fine

Figure C.2: Velocity vectors in T-mixer, each vector indicates the velocity in a cell, but not all vectors are shown.

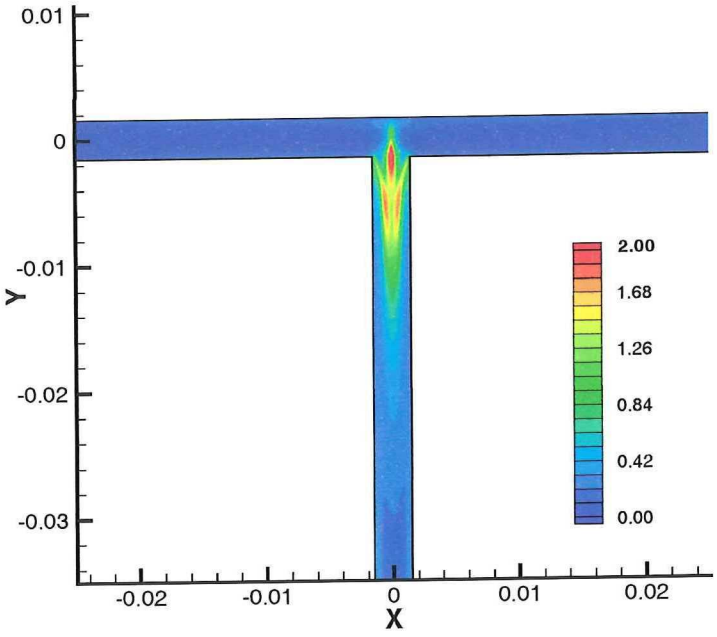

(a) Standard

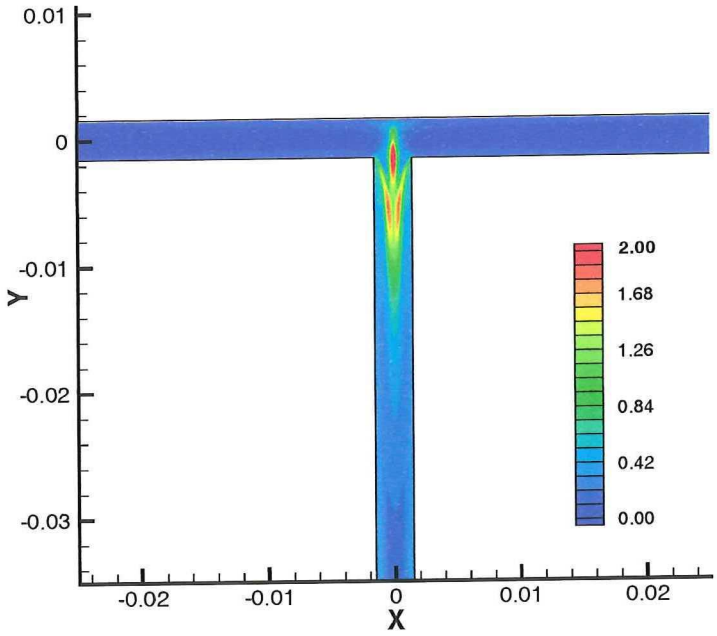

(b) Fine

Figure C.3: Kinetic energy in T-mixer.

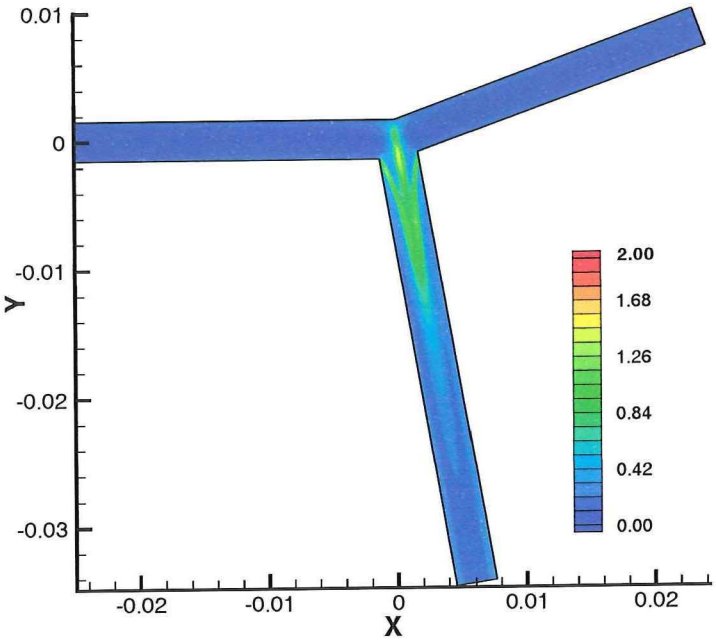

(a) Standard

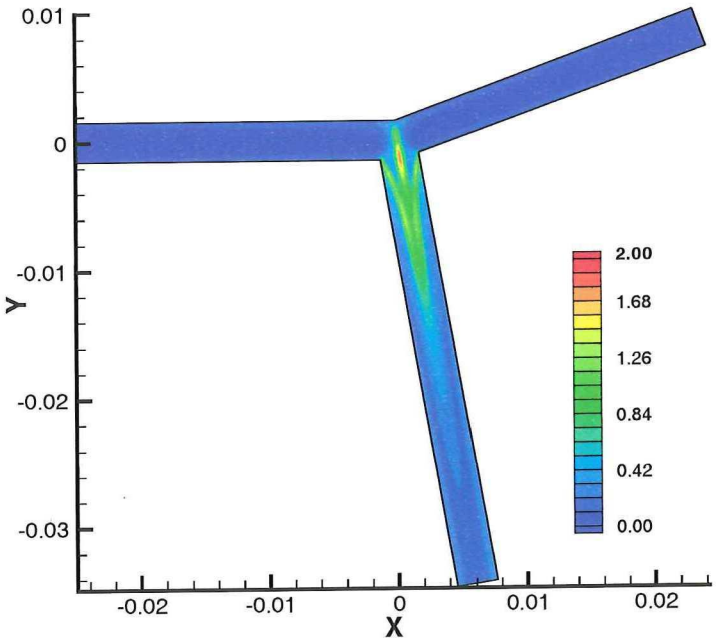

(b) Fine

Figure C.4: Kinetic energy in Y-mixer.

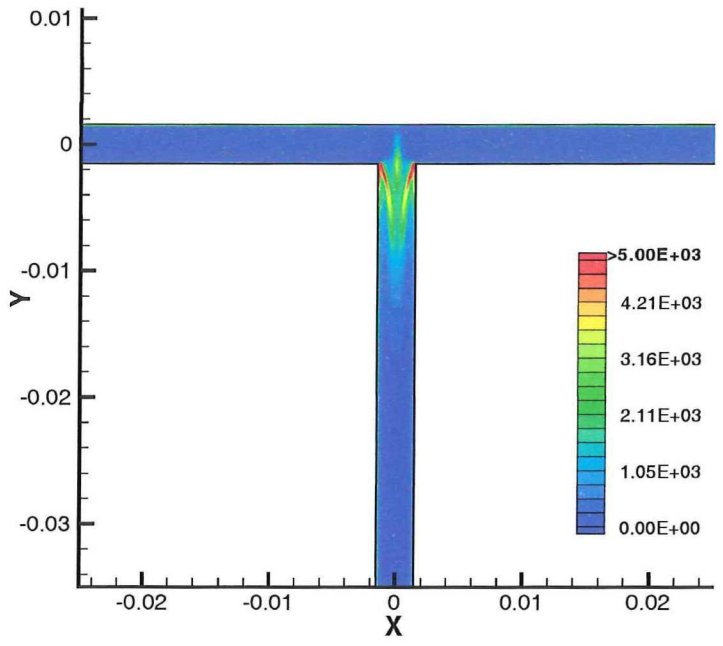

(a) Standard

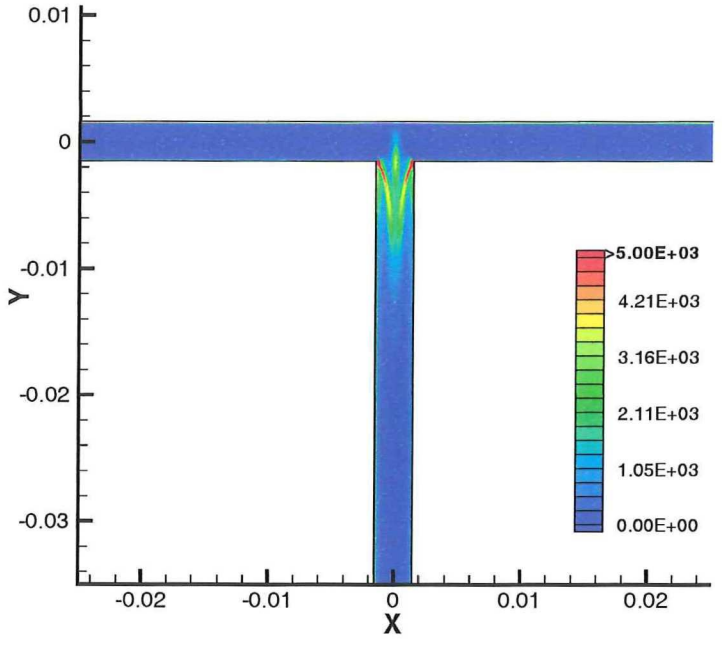

(b) Fine

Figure C.5: Energy dissipation in T-mixer.

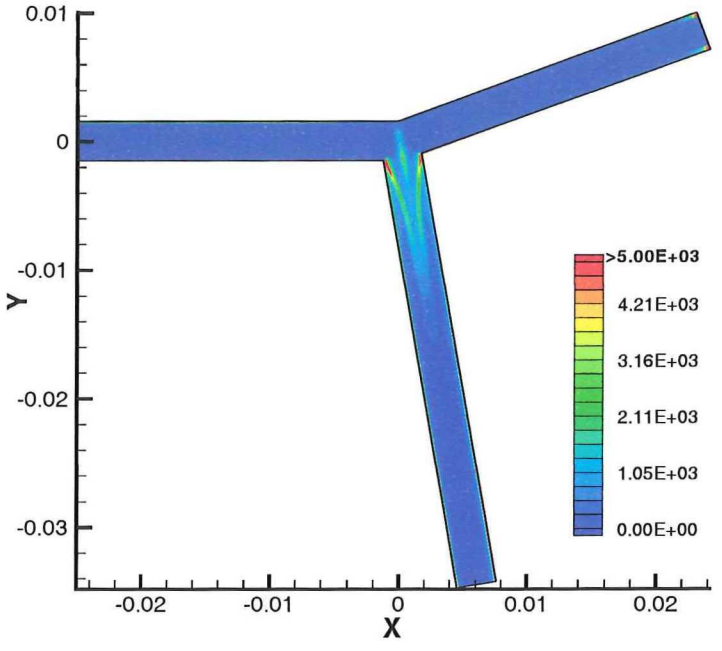

(a) Standard

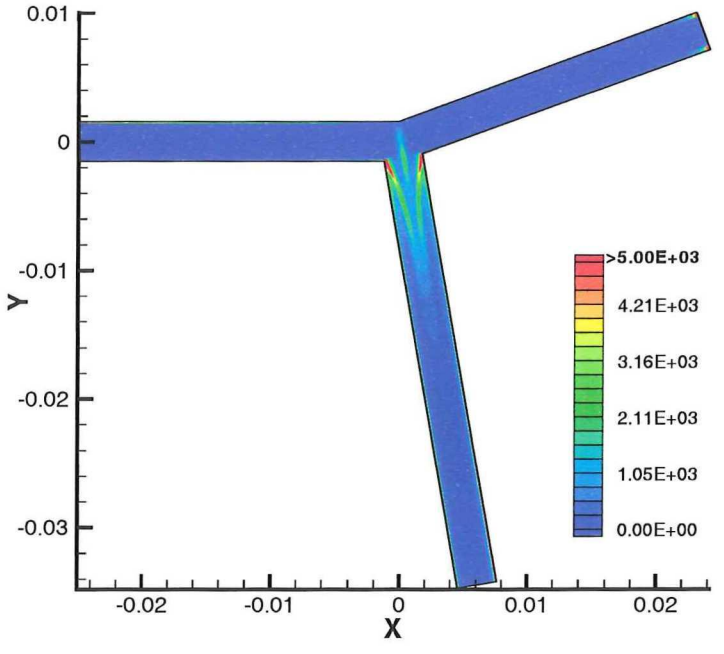

(b) Fine

Figure C.6: Energy dissipation in Y-mixer.

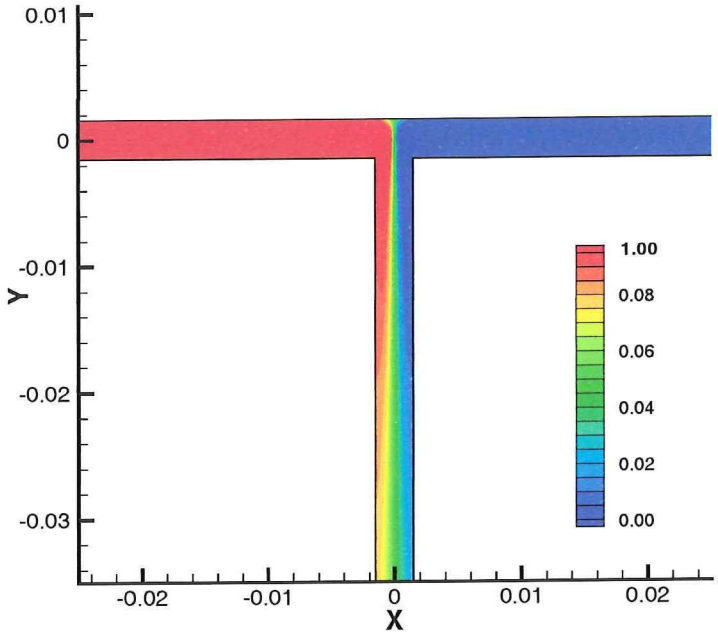

(a) Standard

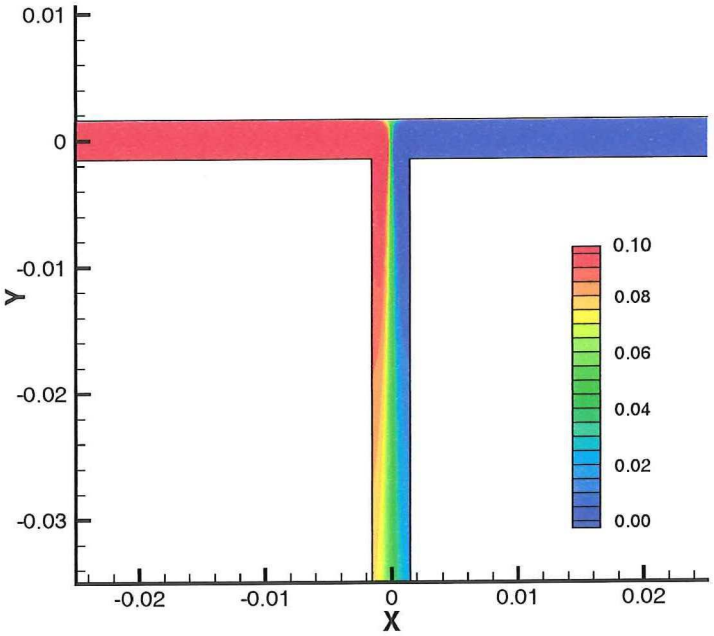

(b) Fine

Figure C.7: Mass fraction of species A in T-mixer.

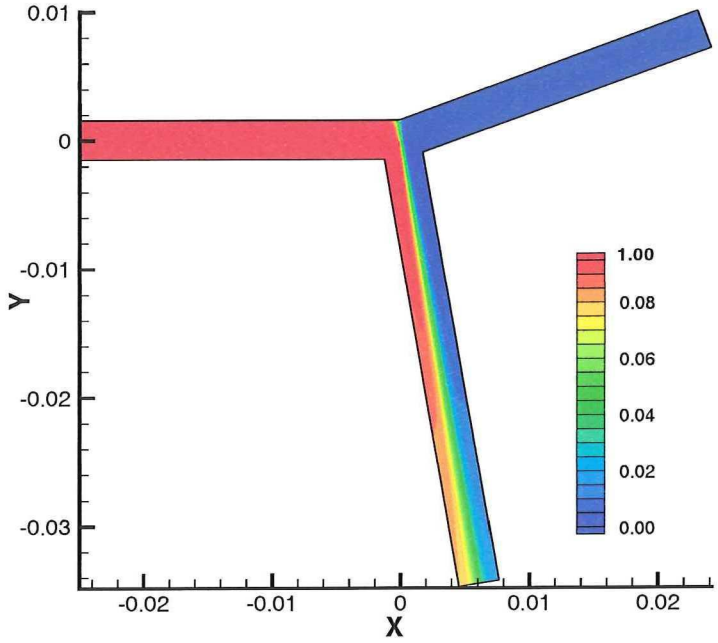

(a) Standard

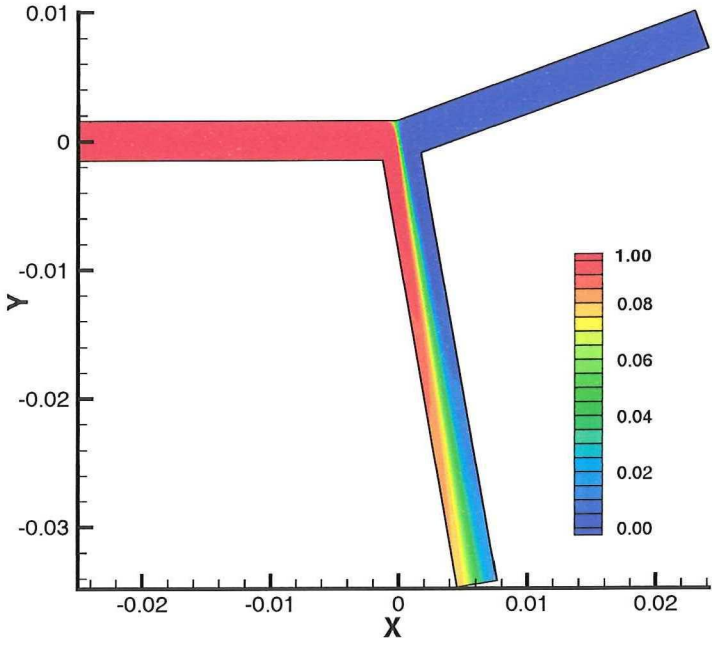

(b) Fine

Figure C.8: Mass fraction of species A in Y-mixer.

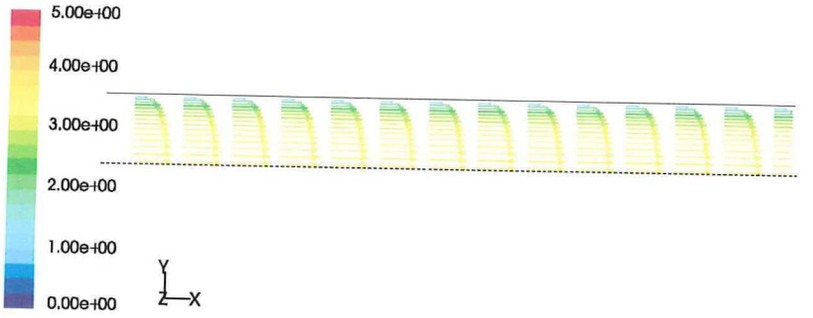

(a) Velocity vectors

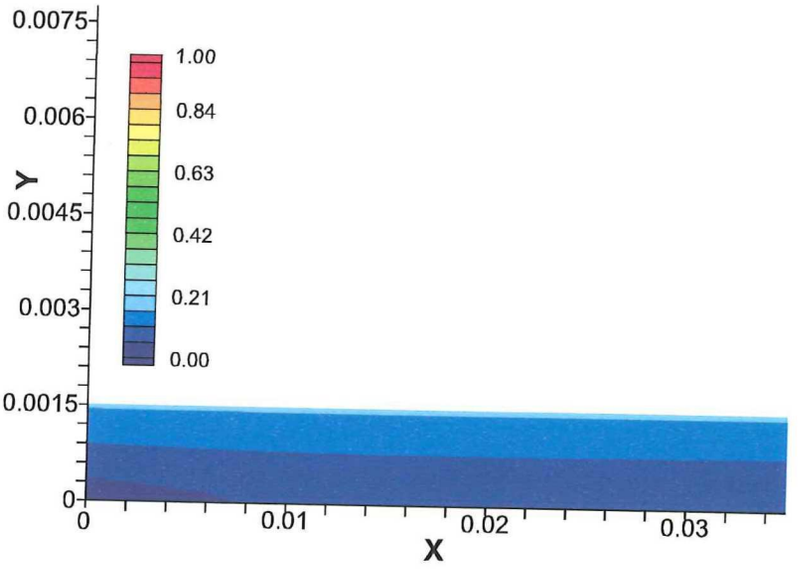

(b) Kinetic energy

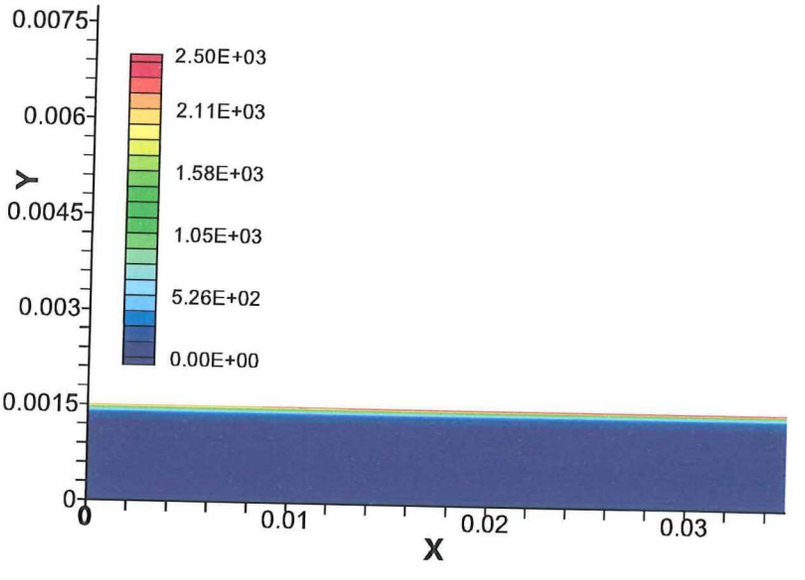

(c) Fine

Figure C.9: Results of pipe flow.

Bibliography

Bałdyga, J., and Bourne, J., 2000, *Turbulent Mixing and Chemical Reactions*: John Wiley and Sons.

Bird, R., Steward, W., and Lightfoot, E., 1960, *Transport Phenomena*: John Wiley and Sons, New York.

Corrsin, S., 1964, The Isotropic Turbulent Mixer: Part II. Arbitrary Schmidt Number: *A.I.Ch.E. Journal*, **10**, 870–877.

Demyanovich, R., and Bourne, J., 1989, Rapid Micromixing by the Impingement of Thin Liquid Sheets. 2. Mixing Study: *Ind. Eng. Chem. Res.*, **28**, 830–838.

Durst, F., Jovanović, J., and Sender, J., 1998, LDA measurements in the near-wall region of a turbulent pipe flow: *J. Fluid Mech.*, **295**, 305–316.

Eble, A., 2000, *Verfahrenstechnik, Precipitation of nanoscale crystals with particular reference to interfacial energy, Dissertation*: Shaker Verlag.

Eggels, J., Unger, F., Weiss, M., Westerweel, J., Adrian, R., Friedrich, R., and Nieuwstadt, F., 1994, Fully developed turbulent pipe flow: a comparison between direct numerical simulation and experiment: *J. Fluid Mech.*, **268**, 175–209.

FluentInc., 1998, *FLUENT 5, User's Guide*:.

Geisler, R., Mersmann, A., and Voit, H., 1988, Makro- und Mikromischen im Rűhrkessel: *Chem.-Ing.-Tech.*, **60**, 947–955.

Hinze, J., 1975, *Turbulence, 2nd Ed.*: McGraw-Hill, New York.

Hrenya, C., Bolio, E., Chakrabarti, D., and Sinclair, J., 1995, Comparison of low Reynolds number k-ϵ turbulence models in predicting fully developed pipe flow: *Chem. Eng. Sci.*, **50**, 1923–1941.

Kim, J., Moin, P., and Moser, R., 1987, Turbulence statistics in fully developed channel flow at low Reynolds number: *J. Fluid Mech.*, **177**, 133–166.

Manth, T., Mignon, D., and Offermann, H., 1996, The role of hydrodyamics in precipitation: *Journal of Crystal Growth*, **166**, 998–1003.

Mohanty, R., Bhandarkar, S., Zuromski, B., Brown, R., and Estrin, J., 2000, Characterizing the Product Crystals from a Mixing Tee Process: *AIChE Journal*, **34**, 2063–2068.

Morsi, S., and Alexander, A., 1972, An Investigation of Particle Trajectories in Two-Phase Flow Systems: *J. Fluid Mech.*, **55**, 193–208.

Nieuwstadt, F., 1998, *Turbulentie, theorie en toepassingen van turbulente stromingen*: Epsilon Uitgaven, Utrecht.

Rielly, C., and Marquis, A., 2001, A particle's eye view of crystallizer fluid mechanics: *Chem. Eng. Sci.*, **56**, 2475–2493.

Shekunov, B., Bałdyga, J., and York, P., 2001, Particle formation by mixing with supercritical antisolvent at high Reynolds numbers: *Chem. Eng. Sci.*, **56**, 2421–2433.

Ståhl, M., Åslund, B., and Å.C. Rasmuson, 2001, Reaction Crystallization Kinetics of Benzoic Acid: *AIChE Journal*, **47**, 1544–1560.

Tan, A., 2001, *Mixing Chambers for Fast Precipitation Reactions, Survey of Mixing Chambers and Their Characteristics (literature review)*: TU Delft.

Thakre, S., and Joshi, J., 2000, CFD Modeling of Heat Transfer in Turbulent Pipe Flows: *AIChE Journal*, **46**, 1798–1812.

Versteegh, H., and Malalasekera, W., 1998, *An introduction to Computational Fluid Dynamics, The Finite Volume Method*: Addison Wesley Longman Ltd, Harlow.